SIAM J. Applied Dynamical Systems
Vol. 18, No. 4, pp. 2267–2302


# Synchronization in Multilayer Networks: When Good Links Go Bad*

Igor Belykh†, Douglas Carter‡, and Russell Jeter§

**Abstract.** Many complex biological and technological systems can be represented by multilayer networks where the nodes are coupled via several independent networks. Despite its significance from both the theoretical and the application perspectives, synchronization in multilayer networks and its dependence on the network topology remain poorly understood. In this paper, we develop a universal connection graph-based method which opens up the possibility of explicitly assessing critical multilayer-induced interactions which can hamper network synchronization. The method reveals striking, counterintuitive effects caused by multilayer coupling. It demonstrates that a coupling which is favorable to synchronization in single-layer networks can reverse its role and destabilize synchronization when used in a multilayer network. This property is controlled by the traffic load on a given edge when the replacement of a lightly loaded edge in one layer with a coupling from another layer can promote synchronization, but a similar replacement of a highly loaded edge can break synchronization, forcing a "good" link to go "bad." This method can be transformative in the highly active research field of synchronization in multilayer engineering and social networks, especially in regard to hidden effects not seen in single-layer networks.

**Key words.** synchronization, multilayer networks, traffic load, network topology

**AMS subject classifications.** 34D06, 34D08, 34D20, 93E20

**DOI.** 10.1137/19M1257123

## 1. Introduction.

Complex networks are common models for many systems in physics, biology, engineering, and the social sciences [59, 2, 46]. Significant attention has been devoted to algebraic, statistical, and graph theoretical properties of networks and their relationship to network dynamics (see the review [21] and references therein). The strongest form of network cooperative dynamics is synchronization, which plays a significant role in the functioning of a wide spectrum of technological and biological networks [22, 25, 32, 35, 63, 50, 45, 24, 30, 43], including adaptive and evolving networks [4, 53, 52, 58, 56, 37, 8, 31, 51].

Despite the vast existence of literature on network dynamics and synchronization, the majority of research activities have been focused on oscillators connected through single-layer networks (one type of coupling) [49, 33, 67, 20, 3, 65, 64, 16, 5, 66, 40, 11, 14, 61, 47, 44, 1, 68, 48]. However, in many realistic biological and engineering systems the units can be coupled via mul-

*Received by the editors April 18, 2019; accepted for publication (in revised form) September 24, 2019; published electronically December 17, 2019.
https://doi.org/10.1137/19M1257123
**Funding:** This work was supported by the National Science Foundation (USA) under grants DMS-1909924 and DMS-1616345 and the U.S. Army Research Office under grant W911NF-15-1-0267.
†Department of Mathematics and Statistics and Neuroscience Institute, Georgia State University, Atlanta, GA 30302-410 (ibelykh@gsu.edu).
‡Department of Mathematics and Statistics, Georgia State University, Atlanta, GA 30302-410 (dcarter15@student.gsu.edu).
§Department of Mathematics and Statistics, Georgia State University, Atlanta, GA 30302-410, and Department of Biomedical Informatics, Emory University, Atlanta, GA 30322 (russell.jeter@outlook.com).

tiple, independent systems and networks. Neurons are typically connected through different types of couplings, such as excitatory, inhibitory, and electrical synapses, each corresponding to a different circuitry whose interplay affects network function [39, 13]. Pedestrians on a lively bridge are coupled via several layers of communication, including people-to-people interactions and feedback from the bridge that can lead to complex pedestrian-bridge dynamics [60, 29, 15, 12]. In engineering systems, examples of independent networks include coupled grids of power stations and communication servers where the failure of nodes in one network can lead to the failure of dependent nodes in another network [23]. Such interconnected networks can be represented by multiplex or multilayer networks [38, 19, 62, 18] which include multiple systems and layers of connectivity. Multilayer-induced correlations can have significant ramifications for the dynamical processes on networks, including the effects on the speed of disease transmission in social networks [26] and the role of redundant interdependencies on the robustness of multiplex networks to failure [54].

Typically, in single-layer networks of continuous time oscillators, synchronization becomes stable when the coupling strength between the oscillators exceeds a threshold value [49, 16]. This threshold depends on the individual oscillator dynamics and the network topology. In this context, a central problem is to determine the critical coupling strength necessary to guarantee the stability of synchronization. The master stability function [49] and the connection graph method [16, 5] are usually used to solve this problem in single-layer networks. Both methods reduce the dimensionality of the problem such that synchronization in a large, complex network can be predicted from the dynamics of the individual node and the network structure.

Synchronization in multilayer networks has been studied in [57, 36, 27, 69]; however, its critical properties and explicit dependence on intralayer and interlayer network structures remain poorly understood. This is in particular due to the inability of the existing eigenvalue methods, including the master stability function [49], to give detailed insight into the stability condition of synchronization, as the eigenvalues, corresponding to connection graphs composing a multilayer network, must be calculated via simultaneous diagonalization of two or more connectivity matrices. Simultaneous diagonalization of two or more matrices is impossible in general, unless the matrices commute [57, 36]. A nice approach based on simultaneous block diagonalization of two connectivity matrices was proposed in [36]. This application of the eigenvalue-based approach allows one to reduce the dimensionality of a large network to a smaller network whose synchronization condition can be used to evaluate the stability of synchronization in the large network. For some network topologies, this technique yields a substantial reduction of the dimensionality; however, this reduction is less significant, in general. The reduced network typically contains weighted positive and negative connections, including self-loops, such that the role of multilayer network topologies and the location of critical edges that control synchronization remain difficult to evaluate.

In this paper, we report significant progress towards removing this obstacle to studying synchronization in multilayer networks. We develop a new general stability approach, called the multilayer connection graph method, which does not depend on explicit knowledge of the spectrum of the connectivity matrices and can handle multilayer networks with arbitrary network topologies, which are out of reach for the existing approaches. An example of a multilayer network in this study is a network of Lorenz systems where some of the oscillators

are coupled through the $x$ variable (first layer), some through the $y$ variable (second layer), and some through both (interlayer connections). Our multilayer connection graph method originates from the connection graph method [16, 5] for single-layer networks; however, this extension is highly nontrivial and requires overcoming a number of technically challenging issues. This includes the fact that the oscillators from two $x$ and $y$ layers in the networks of Lorenz systems are connected through the intrinsic, nonlinear equations of the Lorenz system. As a result, multilayer networks can have drastically different synchronization properties from those of single-layer networks. In particular, our method shows that an interlayer traffic load on an edge (in the sense of paths utilizing this edge) is the crucial quantity which can be used to foster or hamper synchronization in a nonlinear fashion. For example, it demonstrates that replacing a link with a light interlayer traffic load by a stronger pairwise converging coupling (a "good" link) via another layer may lower the synchronization threshold and improve synchronizability. At the same time, such a replacement of a highly loaded link can make the network unsynchronizable, forcing the pairwise stabilizing "good" link to go "bad."

The layout of this paper is as follows. First, in section 2, we present and discuss the network model. In section 3, we start with a motivating example of how the replacement of some links in a multilayer network can improve or break network synchronization. In section 4, we formulate the multilayer connection graph method for predicting synchronization in multilayer networks. In sections 5–7, we show how to apply the general method to specific network topologies. In section 8, a brief discussion of the obtained results is given. Finally, the appendix contains the complete derivation of the general method. MATLAB code for algorithms used for calculating network traffic loads is given in the supplementary materials (M125712_01.zip [local/web 230KB]), linked from the main article webpage.

**2. Network model and problem statement.** We start with a network of $n$ oscillators with three connectivity layers:

$$\frac{d\mathbf{x}_i}{dt} = \mathbf{F}(\mathbf{x}_i) + \sum_{j=1}^{n} c_{ij} P \mathbf{x}_j + \sum_{j=1}^{n} d_{ij} L \mathbf{x}_j + \sum_{j=1}^{n} g_{ij} M \mathbf{x}_j, \quad i = 1, \dots, n, \tag{2.1}$$

where $\mathbf{x}_i = (x_i^1, \dots, x_i^s)$ is the state vector containing the coordinates of the $i$th oscillator, $\mathbf{F} : \mathbb{R}^s \to \mathbb{R}^s$ describes the oscillators' individual dynamics, and $C = (c_{ij})$, $D = (d_{ij})$, and $G = (g_{ij})$ are $n \times n$ Laplacian connectivity matrices with zero-row sums and nonnegative off-diagonal elements $c_{ij} = c_{ji}$, $d_{ij} = d_{ji}$, and $g_{ij} = g_{ji}$, respectively [16]. These connectivity matrices $C$, $D$, and $G$ define three different connection layers (also denoted by $C$, $D$, and $G$ with $m$, $l$, and $q$ edges, respectively). The inner matrices $P$, $L$, and $M$ determine which variables couple the oscillators within the $C$, $D$, and $G$ layers, respectively. Without loss of generality, we will be considering oscillators of dimension $s = 3$ with $\mathbf{x}_i = (x_i, y_i, z_i)$. Therefore, the $C$ graph with the inner matrix $P = \mathrm{diag}(1, 0, 0)$ will correspond to the first-layer connections via $x$, the $D$ graph with the inner matrix $L = \mathrm{diag}(0, 1, 0\ )$ will indicate the second-layer connections via $y$, and the graph $G$ with the matrix $M = \mathrm{diag}(0, 0, 1)$ will represent the third-layer connections via $z$. Overall, the oscillators of the network are connected through a combination of the three layers. The graphs are assumed to be undirected [16]. Oscillators, comprising the network (2.1), can be periodic or chaotic. As chaotic oscillators are difficult to synchronize, they are usually used as test bed examples for probing the effectiveness of a

given stability approach. However, we will show that the chaoticity of the oscillators is not important for the nonintuitive effects of multilayer synchronization. The oscillators used in the numerical verification of our stability method are chaotic Lorenz [41], chaotic double-scroll [42], and periodic Hindmarsh–Rose [34].

In this paper, we are interested in the stability of complete synchronization defined by the synchronization manifold $S = \{\mathbf{x}_1(t) = \mathbf{x}_2(t) = \cdots = \mathbf{x}_n(t) = \mathbf{s}(t)\}$, where the synchronous solution $\mathbf{s}(t) = (x(t), y(t), z(t))$ is governed by the uncoupled individual oscillator. Our main objective is to determine a threshold value for the coupling strengths required for the stability of the synchronization manifold $S$. We seek to predict this threshold or the absence thereof in the general network (2.1) from synchronization in the simplest two-node network and graph properties of the multilayer network structures.

Based on their synchronization properties and the way they are coupled, oscillators can be divided into three main types [21]. Type I oscillators are capable of synchronizing globally and retaining synchronization for any coupling strengths exceeding the synchronization threshold. Most known oscillators, including the Lorenz, double-scroll, and Hindmarsh–Rose oscillators belong to Type I systems. A much narrower Type II class of oscillators contains $x$-coupled Rössler systems [49] in which synchronization becomes stable but eventually loses its stability with an increase of coupling [33]. Type III oscillators cannot be synchronized by a given choice of coupling. In this work, we limit our consideration to the large class of Type I networks; however, an extension of our method to Type II networks could be performed with moderate effort and remains a subject of future study.

**3. A motivating example and a puzzle.** To illustrate the complexity of assessing multilayer connections and their controversial role in fostering or hindering synchronization, we begin with simple two-layer networks of chaotic Lorenz oscillators, depicted in Figure 1(a)–(c). The two-layer networks are chosen as a minimum model which can exhibit counterintuitive effects due to the multilayer structure. For the two-layer networks of Lorenz oscillators, the vector equation (2.1) can be written in a more reader-friendly scalar form:

$$\begin{aligned} \dot{x}_i &= \sigma(y_i - x_i) + \sum_{j=1}^{n} c_{ij} x_j, \\ \dot{y}_i &= r x_i - y_i - x_i z_i + \sum_{j=1}^{n} d_{ij} y_j, \\ \dot{z}_i &= -b z_i + x_i y_i, \quad i = 1, \ldots, n, \end{aligned} \tag{3.1}$$

where the connectivity matrix $C = (c_{ij})$ describes the topology of $x$ connections (black edges in Figure 1(a)–(c)), and matrix $D = (d_{ij})$ describes the location of one $y$ edge (blue or red edge). Notice the absence of the $z$ coupling and, therefore, of the third layer $G$. The parameters of the individual Lorenz oscillator are standard: $\sigma = 10$, $r = 28$, and $b = 8/3$. The strengths of the $x$ and $y$ coupling are homogeneous ($c_{ij} = c$, $d_{ij} = d$) and varied uniformly ($c = d$).

We are interested in the question of how the replacement of an $x$ edge in the network of Figure 1(a) with a $y$ edge can affect synchronization. To address this question, we first need to understand synchronization properties of two-node single-layer networks of $x$-coupled and $y$-coupled Lorenz systems. It is well known that if the coupling in a single-layer network

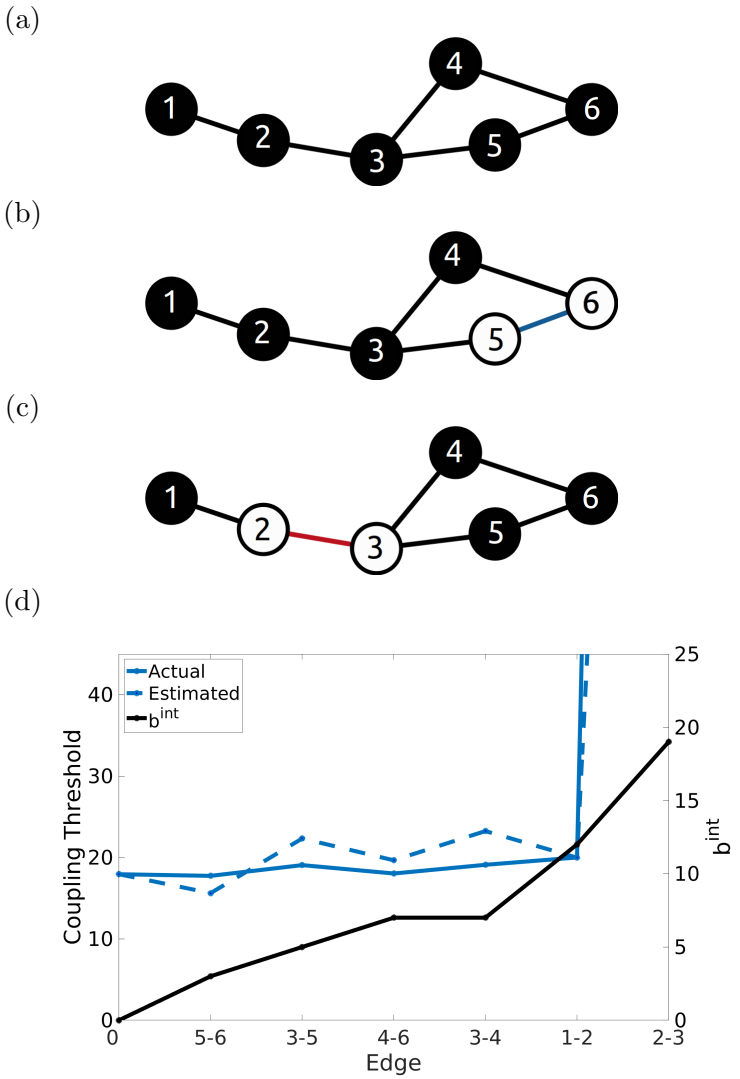


**Figure 1.** *The puzzle: why do "good" links go "bad"? Synchronization in six-node networks of Lorenz systems* (3.1). (a) *Single-layer network, with all $x$ edges (black).* (b) *The replacement of $x$ edge* 5-6 *with a presumably better converging $y$ coupling (blue) improves synchronization, as expected (see* (d)*).* (c) *A similar replacement of $x$ edge* 2-3 *with a $y$ edge (red) makes synchronization impossible by pushing the threshold to infinity (see* (d)*).* (d). *Systematic study of the coupling threshold $c^*$ as a function of the $y$ edge location that replaces an $x$ edge in the original $x$-coupled network* (a). *The blue solid line indicates numerically calculated thresholds. The black solid line depicts the interlayer traffic $b^{int}$ for the respective $y$ edge. Note a significant increase of $b^{int}$ that causes the network to become unsynchronizable as predicted by the method. The predicted coupling thresholds (blue dotted line) are computed from* (4.12) *using the exponential fit in Figure* 3 *and scaling factors $\beta = 0.3517$ and $\gamma = 0.7180$.*

(3.1) with either all $x$ or all $y$ connections exceeds a critical threshold, then synchronization becomes stable and persists for any $c > c*$ and $d > d^*$, respectively [16].

Calculated numerically,[1] these coupling thresholds are $c^* \approx 3.81$ for the two-node $x$-coupled network and $d^* \approx 1.42$ for the $y$-coupled network. As the synchronization threshold $d^*$ is significantly lower, one could expect that replacing an $x$ edge with a presumably better converging $y$ coupling improves synchronization. This is true for the network in Figure 1(b) when $x$ edge 5-6 is replaced with a $y$ edge, yielding a minor reduction in the synchronization threshold from $c^* \approx 17.94$ in the single-layer $x$-coupled network in Figure 1(a) to $c^* \approx 17.74$ in the multilayer network in Figure 1(b). The network of Figure 1(c) replaces an $x$ edge with a $y$ edge, and naturally we would expect this to improve synchronization. Surprisingly, the contrary is true—this action makes the network unsynchronizable (see the coupling threshold jumping to infinity in Figure 1(d)).

What is the origin of this counterintuitive effect? Why do edges in a multilayer network reverse their stabilizing roles depending on the edge location whereas they are well behaved in single-layer networks? The connectivity matrices for $x$ and $y$ coupling in the networks in Figures 1(b) and 1(c) do not commute and, therefore, the predictive power of the master stability function–based methods [57, 36, 27] is severely impaired. This puzzle calls for an explanation and ultimately motivates the development of an effective, general method for assessing the stability of synchronization in multilayer networks.

In the following, we will develop such a method that identifies the location of critical interlayer links which control stable synchronization and reveals its explicit dependence on an interlayer traffic load on a given edge.

## 4. Multilayer connection graph method.

In this section, we present the analytical method and then derive its practical numerically assisted version, which represents an effective approach to assessing the role of critical links from the knowledge of two-node networks and graph characteristics of the underlying network topology. We then demonstrate how to apply the method to specific network configurations.

### 4.1. Analytical method: Conservative bounds.

To formulate the main theorem, we first need to make several assumptions and introduce important quantities. Towards assessing the role of the individual oscillator and type of pairwise coupling within each layer, we should consider three types of the two-node networks (2.1) which are only coupled through one variable. These are $x$-coupled, $y$-coupled, and $z$-coupled networks. For each of these two-node networks with coupling strengths $c_{12} = c_{21} = c$, $d_{12} = d_{21} = d$, and $g_{12} = g_{21} = g$, respectively, we assume that there exists a threshold value, $c^*$ for the $x$-coupled, $d^*$ for the $y$-coupled, and $g^*$ for the $z$-coupled network, which guarantees the global stability of synchronization for any coupling strength exceeding the threshold values. This assumption implies that each $x$, $y$, and $z$ coupling belongs to the Type I class of coupled oscillators. For mathematical convenience, we introduce the corresponding constants $a_x = 2c^*$, $a_y = 2d^*$, and $a_z = 2g^*$, which are the double coupling strengths that are sufficient for the synchronization in the $x$-, $y$-, and $z$-coupled two-node networks, respectively. Rigorous upper bounds on the double coupling strength $a_x$ explicit in parameters of the individual oscillator have been previously derived for

[1] Numerical calculations of coupling thresholds $c^*$ and $d^*$ throughout this paper were performed using an eighth-order Runge–Kutta method with step size $h = 0.001$. Initial conditions for $(x_i, y_i, z_i)$ are chosen uniformly at random within the unit hypersphere. Synchronization has been defined as the sum of all difference variables less than 0.00001.

coupled Lorenz oscillators [16], double-scroll Chua oscillators [17], driven nonlinear pendulums [10], and Hindmarsh–Rose neuron models [11].

We also consider the two-node network with all $x$, $y$, and $z$ coupling and introduce the triple $(\omega_x, \omega_y, \omega_z)$ as a combination of the double coupling strengths $c$, $d$, and $g$ that guarantee the synchronization in the $xyz$-coupled two-node network. These constants are such that $\omega_x \leq a_x$, $\omega_y \leq a_y$, and $\omega_z \leq a_z$, where equality relates to the previous case of the two-node network coupled through one variable. Obviously, there are different possible combinations of $\omega_x$, $\omega_y$, and $\omega_z$ to choose from; however, one should pick a combination that balances out the stability conditions. This point will be discussed in the next subsection in more detail.

Similarly to the connection graph method for single-layer networks [16], we also need to introduce graph theoretical quantities that characterize the total length of the chosen paths that go through each edge of the three-layer network (2.1). This is done by choosing a set of paths $\{|P_{ij}|\ i, j = 1, \ldots, n,\ j > i\}$, one for each pair of nodes $i, j$, and then determining their lengths $|P_{ij}|$, the number of edges in each $P_{ij}$. We then partition the chosen paths into two categories, such as (i) the paths within one layer that only contain edges of one coupling type, for example $x$ edges, and (ii) the paths that are composed of two or three types of edges, for example $x$ and $y$ edges. Starting from the first $x$ layer $C$, we calculate the following quantity for each $x$ edge $k = 1, \ldots, m$:

$$b_k^x = \sum_{j>i;\ k \in P_{ij} \in C}^{n} |P_{ij}|. \tag{4.1}$$

Here, $b_k^x$ is the sum of the lengths of all chosen paths $P_{ij}$ between any pair of nodes $i$ and $j$ which belong to the $x$ layer $C$ and go through a given $x$ edge $k$. These paths are entirely composed of $x$ edges. Similarly, we introduce

$$b_k^y = \sum_{j>i;\ k \in P_{ij} \in D}^{n} |P_{ij}|,\ k = 1, \ldots, l, \quad b_k^z = \sum_{j>i;\ k \in P_{ij} \in G}^{n} |P_{ij}|,\ k = 1, \ldots, q, \tag{4.2}$$

as the sums of all chosen paths $P_{ij}$ between any pair of nodes $i$ and $j$ which entirely belong to the $y$ ($z$) layer and go through a given $y$ ($z$) edge $k$. Finally, we introduce the quantity

$$b_k^{int} = \sum_{j>i;\ k \in P_{ij}:(i,j) \notin C,D,G} |P_{ij}| \tag{4.3}$$

as the sum of the lengths of all chosen paths $P_{ij}$ which pass through a given edge $k$ and are composed from more than one type of edges. These are the paths between pairs of nodes $i$ and $j$ which belong to two different layers. For example, a path between two nodes from $x$ and $y$ layers is typically composed of $x$ and $y$ edges but may also contain $z$ edges as the path from a node from the $x$ layer may have to pass through the $z$ layer to reach the $y$ layer.

In terms of traffic networks, the graph theoretical quantities $b_k^x$, $b_k^y$, $b_k^z$, and $b_k^{int}$ represent the total lengths of the chosen roads that go through a given edge $k$ which can be loosely analogized as a busy street. Therefore, we refer to them as "traffic" loads. In this view, the quantity $b_k^{int}$ is a traffic load on edge $k$, caused by interlayer travelers.

Having introduced the main constants $a_x$, $a_y$, $a_z$, $\omega_x$, $\omega_y$, $\omega_z$, related to the two-node network (2.1) and the traffic loads $b_k^x$, $b_k^y$, $b_k^z$, and $b_k^{int}$, we can formulate the multilayer connection graph method. For convenience, we use the notations $c_k = c_{i_k,j_k}$, $d_k = d_{i_k,j_k}$, and $g_k = g_{i_k,j_k}$, which indicate the coupling strengths of the corresponding edges $k$ on the $x$, $y$, and $z$ layer graphs, respectively.

Theorem 4.1 (sufficient conditions). *Complete synchronization in the three-layer network* (2.1) *is globally stable if for each edge* $k$

$$\begin{array}{l} c_k > \frac{1}{n}\left\{a_x \cdot b_k^x + \omega_x \cdot b_k^{int} + \alpha_x^k\right\},\ k = 1, \ldots, m, \\ d_k > \frac{1}{n}\left\{a_y \cdot b_k^y + \omega_y \cdot b_k^{int} + \alpha_y^k\right\},\ k = 1, \ldots, l, \\ g_k > \frac{1}{n}\left\{a_z \cdot b_k^z + \omega_z \cdot b_k^{int} + \alpha_z^k\right\},\ k = 1, \ldots, q, \end{array} \tag{4.4}$$

*where the constants* $\alpha_x^k$, $\alpha_y^k$, *and* $\alpha_z^k$ *are chosen large enough such that they can globally stabilize the auxiliary stability systems written for the difference variables that correspond to an edge* $k : \mathbf{X}_k = \mathbf{X}_{ij} = \mathbf{x}_j - \mathbf{x}_i$*:*

$$\begin{aligned} \text{for } \alpha_x^k: \quad \dot{\mathbf{X}}_k &= \left[\int_0^1 D\mathbf{F}(v\mathbf{x}_j + (1-v)\mathbf{x}_i)dv\right]\mathbf{X}_k \\ &+\omega_y b_k^{int} L\mathbf{X}_k + \omega_z b_k^{int} M\mathbf{X}_k - (a_x + \alpha_x^k)P\mathbf{X}_k, \end{aligned} \tag{4.5}$$

$$\begin{aligned} \text{for } \alpha_y^k: \quad \dot{\mathbf{X}}_k &= \left[\int_0^1 D\mathbf{F}(v\mathbf{x}_j + (1-v)\mathbf{x}_i)dv\right]\mathbf{X}_k \\ &+\omega_x b_k^{int} P\mathbf{X}_k + \omega_z b_k^{int} M\mathbf{X}_k - (a_y + \alpha_y^k)L\mathbf{X}_k, \end{aligned} \tag{4.6}$$

$$\begin{aligned} \text{for } \alpha_z^k: \quad \dot{\mathbf{X}}_k &= \left[\int_0^1 D\mathbf{F}(v\mathbf{x}_j + (1-v)\mathbf{x}_i)dv\right]\mathbf{X}_k \\ &+\omega_x b_k^{int} P\mathbf{X}_k + \omega_y b_k^{int} L\mathbf{X}_k - (a_z + \alpha_z^k)M\mathbf{X}_k, \end{aligned} \tag{4.7}$$

*where* $D\mathbf{F}$ *is the* $s \times s$ *Jacobian matrix of* $\mathbf{F}$ *and the notation* $\int_0^1 D\mathbf{F}(v\mathbf{x}_j + (1-v)\mathbf{x}_i)dv$ *represents the mean value theorem applied to the difference of vector functions* $\mathbf{F}(\mathbf{x}_j) - \mathbf{F}(\mathbf{x}_i)$.

*Proof.* The proof closely follows the notations and steps in the derivation of the connection graph method [16] for single-layer networks up to a point where the stability argument becomes drastically different and yields the new terms $\omega_x b_k^{int}$, $\omega_y b_k^{int}$, and $\omega_z b_k^{int}$, which play a pivotal role in synchronization of multilayer networks. The complete proof is given in the appendix. ∎

*Remark* 1. It is important to notice that positive terms $+\omega_y b_k^{int} L\mathbf{X}_k$ and $+\omega_z b_k^{int} M\mathbf{X}_k$ in (4.5), $+\omega_x b_k^{int} P\mathbf{X}_k$ and $+\omega_z b_k^{int} M\mathbf{X}_k$ in (4.6), and $+\omega_x b_k^{int} P\mathbf{X}_k$ and $+\omega_y b_k^{int} L\mathbf{X}_k$ in (4.7) play a destabilizing role such that a heavily loaded edge with a high $b_k^{int}$ can represent a potential problem for making the systems (4.5)–(4.7) stable at all. This observation has dramatic consequences for synchronization in specific multilayer networks described in the following sections and also is a key to solving the puzzle of Figure 1.

*Remark* 2. If all $x$, $y$, and $z$ connection graphs are connected such that all oscillators are coupled via all three graphs, the stability of synchronization can be simply assessed by

applying the connection graph method [16] for each of the $x$, $y$, and $z$ connected graphs and combining the three conditions as follows: $c_k + d_k + g_k > \frac{1}{n}\left\{a_x b_k^x + a_y b_k^y + a_z b_k^z\right\}$ (cf. the condition (9.25) in the appendix). As a result, one should not expect the effects due to the multilayer coupling discussed in the motivating example.

*Remark* 3. The stability criterion (4.4) can be directly extended to oscillators of higher dimensions and/or multiple connection layers. For example, in the case of a four-layer network of five-dimensional oscillators with variables $x, y, z, u, w$ coupled through the first four variables $x, y, z, u$, the stability criterion (4.4) should be simply extended by adding a similar inequality for the coupling strength corresponding to edges from the fourth additional layer with $a_u$, $b_k^u$, $\omega_u$, and $\alpha_u^k$ defined similarly to the constants corresponding to the $x$, $y$, and $z$ variables. The remaining uncoupled variable $w$ does not play an explicit role in the stability criterion; however, it affects (i) the choice of values for $\omega_x$, $\omega_y$, $\omega_z$, $\omega_u$ required for synchronization in the two node $xyzu$-coupled network and (ii) the values of $\alpha_x^k, \alpha_y^k, \alpha_z^k, \alpha_u^k$ via the increased dimensionality of the four auxiliary systems similar to (4.5)–(4.7).

While the stability criterion (4.4) is completely rigorous, the theoretical bounds derived by using Lyapunov functions may give large overestimates on the threshold coupling strength. As a result, bounds of the constants $\alpha_x^k$, $\alpha_y^k$, and $\alpha_z^k$ that are required to stabilize the auxiliary systems (4.5)–(4.7) may be too conservative or not exist.

In the following subsection, we take a more practical route towards developing a semi-analytical approach which evaluates local stability of synchronization. This computer-assisted version of the method combines numerically calculated constants associated with the individual oscillator dynamics with graph theoretical quantities such as traffic loads. In this way, this method combines the best of both worlds—the master stability function and the developed connection graph–based method—and becomes an effective, predictive tool for the general multilayer network (2.1) where the synchronization threshold or the absence thereof can be deduced from the properties of the individual oscillators and the network topologies of the connection layers.

**4.2. Numerically assisted multilayer connection graph method.** For the sake of clarity, we consider the general network (2.1) with only two connection layers $C$ and $D$. Its general vector equation (2.1) can be rewritten in the scalar form

$$\begin{aligned} \dot{x}_i &= F(x_i, y_i, z_i) + \sum_{j=1}^{n} c_{ij} x_j, \\ \dot{y}_i &= Q(x_i, y_i, z_i) + \sum_{j=1}^{n} d_{ij} y_j, \\ \dot{z}_i &= R(x_i, y_i, z_i), \quad i = 1, \ldots, n, \end{aligned} \tag{4.8}$$

with $\mathbf{x}_i = (x_i, y_i, z_i)$ and $\mathbf{F} = (F(x_i, y_i, z_i), Q(x_i, y_i, z_i), R(x_i, y_i, z_i))$.

The stability conditions (4.4) can be directly adapted to the two-layer network (4.8) by only considering the two first inequalities for $c_k$ and $d_k$ with $\alpha_x^k$ and $\alpha_y^k$ calculated via the auxiliary systems (4.5) and (4.6) without the terms containing the projection matrix $M$. Computer-assisted derivation of the stability conditions (4.4) for the network (4.8) is a four-step process which can be summarized as follows.

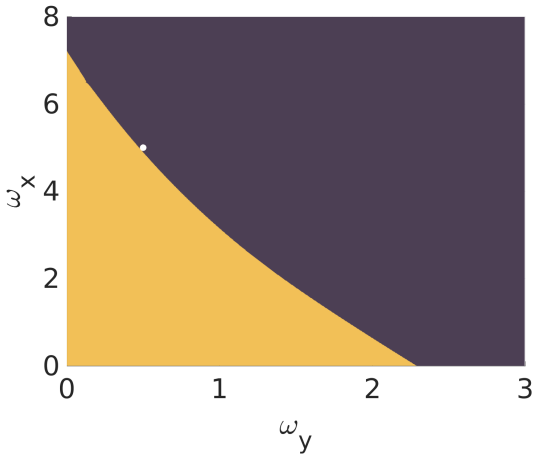


**Figure 2.** *Stability of synchronization in a two-node network of xy-coupled Lorenz systems (3.1) as a function of the x coupling, $\omega_x$, and the y coupling, $\omega_y$. Yellow depicts instability (nonzero synchronization error), and purple depicts stability (zero synchronization error). The white dot indicates the pair $(\omega_x, \omega_y)$ used in the predictions shown in Figures 1(d) and 4(c).*

*Step* 1: *Synchronization thresholds in a two-node network.* Calculate a stability diagram for synchronization in the simplest two-node $xy$-coupled network with $c_{12} = c_{21} = c$ and $d_{12} = d_{21} = d$, using the variational equations for infinitesimal transverse perturbations $\xi = x_2 - x_1$, $\eta = y_2 - y_1$, and $\zeta = z_2 - z_1$:

$$\begin{aligned} \dot{\xi} &= F_x(\mathbf{s})\xi + F_y(\mathbf{s})\eta + F_z(\mathbf{s})\zeta - 2c\xi, \\ \dot{\eta} &= Q_x(\mathbf{s})\xi + Q_y(\mathbf{s})\eta + Q_z(\mathbf{s})\zeta - 2d\eta, \\ \dot{\zeta} &= R_x(\mathbf{s})\xi + R_y(\mathbf{s})\eta + R_z(\mathbf{s})\zeta. \end{aligned} \tag{4.9}$$

Here, the partial derivatives form the Jacobian $D\mathbf{F}$ as in (4.5) and are evaluated at the synchronous solution $\mathbf{s}(t) = (x(t), y(t), z(t))$.

Use the stability diagram to determine threshold coupling strengths that guarantee stable synchronization in (i) the two-node $x$-coupled network with $c^* = a_x/2$ and $d = 0$; (ii) the two-node $y$-coupled network with $d^* = a_y/2$ and $c = 0$; and (iii) the two-node $xy$ network with $c^* = \omega_x$ and $d^* = \omega_y$ (see Figure 2). The new constants $a_x$ and $a_y$ are double coupling strengths required for synchronization in the two $x$-coupled and $y$-coupled oscillators (4.8), respectively. Note that different combinations of $c = \omega_x$ and $d = \omega_y$ in the $xy$-coupled network can yield stable synchronization. The choice of the pair $(\omega_x, \omega_y)$ is somewhat arbitrary; however, it dictates the choice of constants in the stability diagrams in Step 3. It is often a good idea to choose $\omega_x$ and $\omega_y$ such that both are nonzero and lie somewhere in the middle range of $(\omega_x, \omega_y)$ to balance out the stability conditions in Step 4.

*Step* 2: *Graph theoretical quantities and traffic loads.* This calculation is similar to that of the connection graph method for single-layer networks [16], except that the traffic load should be partitioned into three groups: intralayer traffic loads $b_k^x$ and $b_k^y$ within the $x$ and $y$ layers, respectively, and interlayer traffic load $b_k^{int}$ between the layers. To do so, we first choose a set of paths $\{|P_{ij}|\ i, j = 1, \ldots, n,\ j > i\}$, one for each pair of vertices $i, j$, and determine their

lengths $|(P_{ij}|$, the number of edges in each $P_{ij}$. Then, for each edge $k$ of the $x$ ($y$) layer graph, we calculate the sum $b_k^x$ ($b_k^y$) of the lengths of all $P_{ij}$ that are composed of only $x$ ($y$) edges and pass through $k$. We repeat the same procedure to calculate the sum $b_k^{int}$ of the lengths of all $P_{ij}$ that contain both $x$ and $y$ edges and pass through $k$. These constants depend on the choice of the paths $P_{ij}$. Usually, one uses the shortest path from vertex $i$ to vertex $j$. Sometimes, however, a different choice of paths can lead to lower bounds [11]. In the following section, we will walk the reader through a detailed calculation of traffic loads $b_k^x$, $b_k^y$ and interlayer $b_k^{int}$ in the six-node networks of Figure 1.

Note that Steps 1 and 2 are quite similar to those one takes when applying the master stability function or the connection graph method to single-layer networks. That is, one identifies the role of the single node (via the calculation of the Lyapunov exponents in Step 1) and the role of the underlying network topology (via the calculation of the traffic loads in Step 2).

The next step is a new component of the method which does not follow from the connection graph method for single-layer networks and allows one to reveal and explain the surprising phenomena, including the previously described puzzle due to the multilayer network structure.

*Step* 3: *Auxiliary stability diagrams to determine* $\alpha_x^k$ *and* $\alpha_y^k$. The auxiliary global stability systems (4.5) and (4.6) for each edge $k$ can be written for the local stability in terms of the variational system (4.9) as follows:

$$\begin{aligned} \dot{\xi} &= F_x(\mathbf{s})\xi + F_y(\mathbf{s})\eta + F_z(\mathbf{s})\zeta - (a_x + \alpha_x^k)\xi, \\ \dot{\eta} &= Q_x(\mathbf{s})\xi + Q_y(\mathbf{s})\eta + Q_z(\mathbf{s})\zeta + A\eta, \\ \dot{\zeta} &= R_x(\mathbf{s})\xi + R_y(\mathbf{s})\eta + R_z(\mathbf{s})\zeta, \end{aligned} \tag{4.10}$$

$$\begin{aligned} \dot{\xi} &= F_x(\mathbf{s})\xi + F_y(\mathbf{s})\eta + F_z(\mathbf{s})\zeta + B\xi, \\ \dot{\eta} &= Q_x(\mathbf{s})\xi + Q_y(\mathbf{s})\eta + Q_z(\mathbf{s})\zeta - (a_y + \alpha_y^k)\eta, \\ \dot{\zeta} &= R_x(\mathbf{s})\xi + R_y(\mathbf{s})\eta + R_z(\mathbf{s})\zeta, \end{aligned} \tag{4.11}$$

where $A = \beta\omega_y b_k^{int}$ and $B = \beta\omega_x b_k^{int}$ with a scaling parameter $\beta$ to be determined.

As in (4.4), the auxiliary stability system (4.10) corresponds to the differences between the nodes connected by an $x$ edge, and (4.11) corresponds to the differences between nodes coupled via a $y$ edge. If the connection layers overlap and the same nodes are connected through both $x$ and $y$ edges, then the auxiliary systems (4.10) and (4.11) should be applied to the corresponding $x$ and $y$ edges independently. Their contributions will then appear in the general stability conditions (see Step 4) for $c_k$ and $d_k$ for the same edge $k$.

Notice that $\alpha_x^k$ [$\alpha_y^k$] must be large enough to stabilize (4.10) [(4.11)] in the presence of the destabilizing term $+A\eta$ [$+B\xi$]. While $a_x = 2c^*$, $a_y = 2d^*$, $\omega_x$, and $\omega_y$ are chosen and fixed in Step 1 (cf. Figure 2), the traffic load $b_k^{int}$ on a given edge $k$ (which is determined in Step 2) controls the choice of $\alpha_x^k$ and $\alpha_y^k$. Thus, if the edge is highly loaded with a large $b_k^{int}$ making $A$ large, then the contribution of the destabilizing term $+A\eta$ in the $\eta$-equation of system (4.10) cannot always be compensated by increasing $\alpha_x^k\xi$ in the $\xi$-equation. Therefore, the auxiliary system (4.10) can become unstable, independently of how large the stabilization coefficient $\alpha_x^k$ is. The same argument relates to the destabilization of the auxiliary system (4.11) via the positive term $+B\xi$.

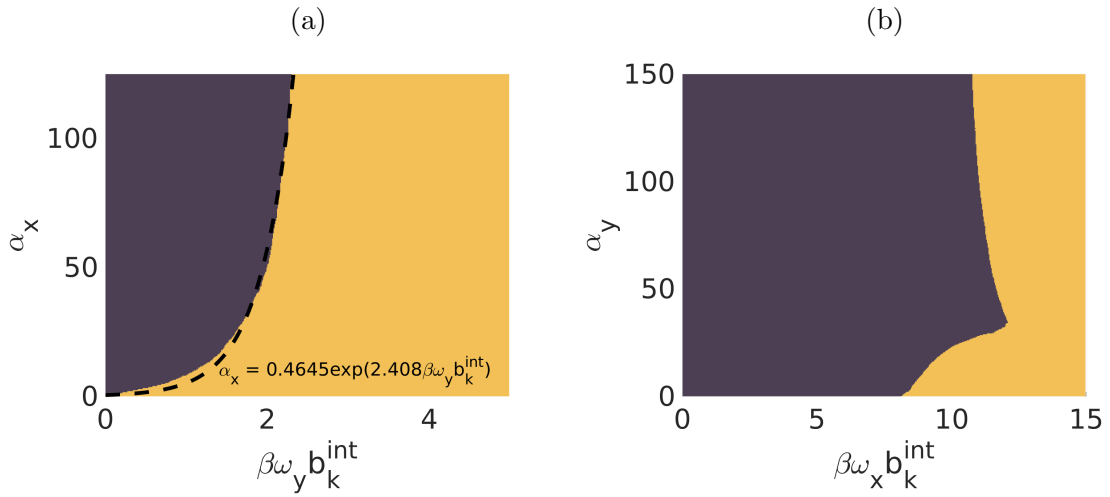


**Figure 3.** *Stability of the auxiliary systems* (5.2) *and* (5.3) *for coupled Lorenz oscillators. Yellow depicts the instability of the origin, while purple indicates its stability. The dependence of the stabilizing term* $\alpha_x$ *on* $\beta\omega_y b_k^{int}$ *is estimated by the exponential function* $\alpha_x = 0.4645 \exp\left(2.408\beta\omega_y b_k^{int}\right)$ *(dashed curve) and is used to predict synchronization thresholds in networks of Figures* 1 *and* 4.

It is important to emphasize that diagrams for the local stability of the two three-dimensional auxiliary systems (4.10) and (4.11) can be calculated once and then be used to identify threshold values for constants $\alpha_x^k$ and $\alpha_y^k$ for each edge $k$ with a given traffic load $b_k^{int}$. To do so, one should calculate the stability diagram for the threshold value of $\alpha_x^k$ $[\alpha_y^k]$ necessary to stabilize the systems (4.10) [(4.11)] as a function of parameter $A$ $[B]$. When generating the diagrams, $A$ and $B$ should be used as free parameters, thereby treating $\beta\omega_y b_k^{int}$ and $\beta\omega_x b_k^{int}$ as single, aggregated control parameters. As a result, the threshold value for $\alpha_x^k$ $[\alpha_y^k]$ required to stabilize the auxiliary system (4.10) [(4.11)] for a given edge $k$ with $b_k^{int}$ can simply be taken from the diagram much in the vein of the master stability function [49] (see Figure 3).

Because of the Cauchy–Schwarz inequality used in the derivation of the analytical method (see the appendix), $b_k^{int}$ provides an overestimate for the terms added to the auxiliary system, we have added the scaling factor $0 < \beta \leq 1$ to $b_k^{int}$ in $A$ and $B$ to compensate for this overestimate. To choose the scaling factor, one can use one point on the threshold value curve for $\alpha_x^k$ or $\alpha_y^k$ (see Figure 3).

*Step* 4: *Putting pieces together.* Using the constants identified in Steps 1–3, we can predict synchronization coupling thresholds for the local stability of synchronization in the multilayer network (4.8) via the numerically assisted modification of (4.4):

$$\begin{aligned} c_k &> \tfrac{1}{n}\left[\gamma_1 a_x \cdot b_k^x + \beta\omega_x \cdot b_k^{int} + \alpha_x^k\right], \\ d_k &> \tfrac{1}{n}\left[\gamma_2 a_y \cdot b_k^y + \beta\omega_y \cdot b_k^{int} + \alpha_y^k\right]. \end{aligned} \tag{4.12}$$

Notice the presence of additional scaling factors $\gamma_1$ and $\gamma_2$ which are chosen to compensate for the conservative nature of $b_k^x$ and $b_k^y$ as in the connection graph stability method for single-layer networks [16, 5]. $\gamma_1$ ($\gamma_2$) scales down the term $\frac{a_x}{n}$ $[\frac{a_y}{n}]$ to match the coupling needed to synchronize the network (4.8) which contains only $x$ edges ($y$ edges) with $b_k^{int} = 0$.

In the case of two-layer networks (4.8) with uniform coupling within each layer $c_k = c$ and $d_k = d$, the stability criterion (4.12) should be satisfied for $c > \max_k c_k$ and $d > \max_k d_k$. The auxiliary systems (4.10) and (4.11) are typically quite sensitive to changes in $A$ and $B$, resulting in large $\alpha_x^k$ or $\alpha_y^k$ that dominate the other two terms in the stability condition (4.12). Therefore, it is often sufficient to check the stability condition (4.12) for only two edges (one from each $x$ and $y$ layer) which have maximum interlayer traffic loads among the edges of the corresponding layers. These maximum traffic loads $\max_k b_k^{int}$ yield the maximum values of $\alpha_x^k$ or $\alpha_y^k$ that in turn maximize the threshold values $c$ and $d$.

Note that the principal new component of our method is the use of the auxiliary stability diagrams which indicate how the dynamics of the given oscillator comprising the network can be stabilized via one variable corresponding to one connection layer when an instability is introduced via the other variable from another connection layer. These stability diagrams are calculated for the three-dimensional variational systems (4.10) and (4.11) and allow for predicting the synchronization threshold in a large multilayer network by using purely graph theoretical quantities, such as traffic loads. In this sense, these diagrams can be viewed as a hybrid of the master stability function and the connection graph method, applied to multilayer networks.

In the following section, we will walk the reader through the implementation of the stability conditions (4.12) for specific two-layer networks and illustrate their implications for the stability of synchronization.

**5. Application of the method: Solving the puzzle.** Armed with the predictive method, we first return to the puzzle to better understand synchronization properties of the six-node networks of Lorenz oscillators (3.1) from Figure 1. Below we follow the four steps of how our numerically assisted method can be applied to these networks.

*Step* 1: *Calculate* $a_x$, $a_y$, $\omega_x$, *and* $\omega_y$. Consider the simplest two-node network (3.1) with both $x$ and $y$ coupling: $c_{12} = c_{21} = c$ and $d_{12} = d_{21} = d$. Use the variational equations (4.9) to determine threshold coupling strengths that guarantee stable synchronization in (i) the two-node $x$-coupled network with $c^* = a_x/2$ and $d = 0$; (ii) the two-node $y$-coupled network with $d^* = a_y/2$ and $c = 0$; and (iii) the two-node $xy$ network with $c^* = \omega_x$ and $d^* = \omega_y$.

The numerically calculated thresholds for the $x$-coupled and $y$-coupled two-node network (3.1) reported in section 3 are $c^* \approx 7.62/2$ and $d^* \approx 2.84/2$, respectively. This yields the double coupling strength constants $a_x = 7.62$ and $a_x = 2.84$ to be used in (4.12).

Note that different combinations of $c = \omega_x$ and $d = \omega_y$ in the $xy$-coupled network yield stable synchronization (see Figure 2). Without loss of generality, we choose $c = \omega_x = 5$ and $d = \omega_y = 0.5$ as a point on the stability boundary in Figure 2 and keep these values fixed for the prediction of the synchronization threshold in larger two-layer networks (3.1) with arbitrary topologies.

*Step* 2: *Calculate traffic loads* $b_k^x$, $b_k^y$, *and* $b_k^{int}$. We use the six-node multilayer network of Figure 1(b) as an example for calculating intralayer traffic loads $b_k^x$ and $b_k^y$ within the $x$ and $y$ layers, respectively, and interlayer traffic load $b_k^{int}$ between the layers. To compute all of the paths that pass through a given edge, it is recommended that the reader algorithmically find the shortest path between every pair of oscillators, and take note of the paths that go through edge $k$ and differentiate the paths that entirely belong to only the $x$ or $y$ layers and the ones

that contain a combination of $x$ and $y$ edges. As a result, we can find each edge's traffic loads as follows:

$$
\begin{aligned}
b_{12}^{x} &= |P_{12}| + |P_{13}| + |P_{14}| + |P_{15}| + |P_{16}| \\
&= 1 + 2 + 3 + 3 + 4 = 13, \\
b_{23}^{x} &= |P_{13}| + |P_{14}| + |P_{15}| + |P_{16}| + |P_{23}| \\
&\quad + |P_{24}| + |P_{25}| + |P_{26}| = 20, \\
b_{34}^{x} &= |P_{14}| + |P_{16}| + |P_{24}| + |P_{26}| + |P_{34}| = 15, \\
b_{35}^{x} &= |P_{15}| + |P_{25}| + |P_{35}| = 6, \quad b_{46}^{x} = |P_{16}| + |P_{46}| = 5, \\
b_{56}^{y} &= |P_{56}| = 1, \quad b_{12}^{int} = 0, \quad b_{23}^{int} = 0, \quad b_{34}^{int} = 0, \\
b_{35}^{int} &= |P_{36}| = 2, \quad b_{46}^{int} = |P_{45}| = 2, \\
b_{56}^{int} &= |P_{36}| + |P_{45}| = 4.
\end{aligned} \tag{5.1}
$$

Note that the maximum interlayer traffic load on this network is fairly low and due to our choice of paths is $b_{56}^{int} = 4$, although it could have also been minimized to zero, provided that all paths to node 6 bypass edge 56.

At the same time, the interlayer traffic load in the network of Figure 1(c) is significantly higher since there are no alternatives to go around the "bottle neck" edge 2-3 when traveling from nodes 1 and 2 to nodes 4, 5, and 6. For the same choice of shortest paths, we get $b_{23}^{int} = 19$. The remaining $b_k^x$, $b_k^y$ for the network of Figure 1(c) can be calculated similarly to (5.1).

*Step* 3: *Determine* $\alpha_x^k$ *and* $\alpha_y^k$. The auxiliary systems (4.10) and (4.11) which play the role of a master stability function for synchronization in two-layer networks of Lorenz systems (3.1) take the form

$$
\begin{aligned}
\dot{\xi} &= \sigma(\eta - \xi) - (a_x + \alpha_x^k)\xi, \\
\dot{\eta} &= (r - z(t))\,\xi - \eta - x(t)\zeta + \beta\omega_y b_k^{int}\eta, \\
\dot{\zeta} &= y(t)\xi + x(t)\eta - b\zeta,
\end{aligned} \tag{5.2}
$$

$$
\begin{aligned}
\dot{\xi} &= \sigma(\eta - \xi) + \beta\omega_x b_k^{int}\xi, \\
\dot{\eta} &= (r - z(t))\,\xi - \eta - x(t)\zeta - (a_y + \alpha_y^k)\eta, \\
\dot{\zeta} &= y(t)\xi + x(t)\eta - b\zeta,
\end{aligned} \tag{5.3}
$$

where $x(t), y(t)$, and $z(t)$ correspond to the synchronous solution and are defined by the uncoupled Lorenz system.

As in the auxiliary systems (4.10) and (4.11), the subscripts $k$ in $\xi$, $\eta$, and $\zeta$ are omitted to indicate that the three-dimensional auxiliary systems (5.2) and (5.3) should be calculated only once and the desired values of $\alpha_x^k$ and $\alpha_y^k$ for an edge $k$ can simply be read off from the stability diagrams (see Figure 3). Notice that if the edge is loaded with a high $b_k^{int}$, then the contribution of the positive term $+\beta\omega_y b_k^{int}\eta$ in the $\eta$-equation of system (5.2) cannot always be compensated by increasing $-\alpha_x^k\xi$ in the $\xi$-equation. Typically, this happens when the positive term exceeds the proper negative linear terms, such as $-\eta$ (technically, through a combination of terms in the Routh–Hurwitz criterion).

The complex relationship between these terms in regard to stabilizing (5.2) and (5.3) is shown in Figure 3. Notice the coefficient $\beta$ on the $\beta\omega_y b_k^{int}$ and $\beta\omega_x b_k^{int}$ axes. The diagrams

of Figure 3 confirm the existence of threshold values for $\beta\omega_y b_k^{int}$ and $\beta\omega_x b_k^{int}$ such that even infinitely large values of $\alpha_x$ and $\alpha^y$ cannot compensate for the caused instability and stabilize systems (5.2) and (5.3).

To better quantify this dependence to be used in predicting synchronization thresholds in networks of Lorenz oscillators, we approximate the stability boundary in Figure 3(a) by the exponential function

$$\alpha_x = 0.4645 \exp\left(2.408\beta\omega_y b_k^{int}\right). \tag{5.4}$$

The stability diagrams of Figure 3 along with Figure 2 account for the role of the individual oscillators composing the networks and the way these oscillators are coupled (through $x$ and $y$ coupling) in the stability of synchronization. These diagrams represent an analogue of the master stability function in single-layer networks [49] and help in solving, once and for all, the question of stability for synchronization in two-layer networks involving the Lorenz oscillator through the criterion (4.12), where the role of multilayer network topologies is assessed via the calculation of pure graph theoretical quantities, as shown in the next step.

*Step* 4: *Putting pieces together to solve the puzzle.* Given the stability diagram of Figure 3 with abrupt threshold dependences of $\alpha_x^k$ and $\alpha_y^k$ on increasing interlayer traffic load $b_k^{int}$, the effect of synchrony breaking when a highly loaded $x$ edge is replaced with a better pairwise stabilizing $y$ (see section 3) is no longer a puzzle and directly follows from the application of our stability method. Actually, in a historical retrospective, we first developed the general method that revealed this and other highly counterintuitive effects due to the multilayer structure and then constructed the network examples. To make the presentation more appealing before it becomes too technical, we have decided to put forward the motivating example. As our exhaustive study of various network configurations suggests, we hypothesize that the six-node networks of Figure 1 are minimum size networks of Lorenz oscillators that exhibit the synchrony breaking phenomenon.

To test the predictive power of our approach with the constants identified in Steps 1–3, we perform a systematic study of how one edge replacement, in which we replace only one $x$ edge in the single-layer, $x$-coupled network of Figure 1(a) with a $y$ edge, affects synchronization. The edge replacement is performed in the order of the increasing interlayer traffic load on this edge, $b_k^{int}$. After computing the coupling threshold required to synchronize the new network, this edge reverts back to being an $x$ edge. This results in multiple networks of five $x$ edges and one $y$ edge. The two multilayer networks of Figures 1(b) and 1(c) with the drastically different synchronization properties are two instances of this replacement process. Figure 1(d) presents the actual synchronization threshold values (blue solid line), the interlayer traffic loads $b^{int}$ (black line) calculated similarly to (5.1), and the threshold values predicted by the numerically assisted criterion (4.4) with constants $a_x = 7.20$, $a_y = 2.63$, $\omega_x = 5.00$, and $\omega_y = 0.50$ chosen above. The constants $\alpha_x^k$ and $\alpha_y^k$ are taken from the diagrams of Figures 3(a) and (b), respectively. As the stability system (5.2) is much more sensitive to the changes in $b_k^{int}$ than (5.3) (cf. the onset of instability in Figures 3(a)–(b)), the threshold values for $c_{ij}$ in the criterion (4.12) for the $x$ layer largely dominate over $d_{ij}$. Thus, since the synchronization threshold for the entire network (3.1) with uniform coupling $c = d$ is defined by the maximum of the thresholds $c_{ij}$ or $d_{ij}$ for each edge of the multilayer graph, the maximum threshold

values predicted by the method and depicted in Figure 1(d) are the ones corresponding to $x$ edges with coupling $c$. These threshold values are calculated using (4.12) as follows:

$$c > \max_k \left\{ c_k = \frac{1}{n} \left[ \gamma a_x \cdot b_k^x + \beta \omega_x \cdot b_k^{int} + \alpha_x^k \right] \right\}, \tag{5.5}$$

where $\alpha_x^k$ is defined by the stability diagram of Figure 3(a) via the approximating function (5.4) for each edge $k$, and $a_x$, $\omega_x$, and $b_k^{int}$ are determined in Steps 1–3. The scaling factor $\gamma$ is chosen to scale down the term $\frac{a_x}{n}$ to match the coupling needed to synchronize the six-node network of Figure 1(a) with only $x$ edges. The scaling factor $\beta$ is then chosen for the network of Figure 1(b) with the lowest $b_k^{int} = 4$ to match the actual synchronization threshold and then kept constant for predicting the thresholds in the other six-node networks with one replaced $x$ edge. Figure 1(d) shows that the predicted thresholds are fairly close to the actual ones, and the criterion (5.5) correctly predicts an increase or decrease of the coupling threshold for each six-node network and ultimately predicts synchrony break for the network with the replaced $x$ edge 2-3.

As Figure 1(d) indicates when lightly loaded edges (edges with fewer chosen paths passing through them) are replaced, the effect on the synchronization stability is fairly small. As discussed in the description of the motivating example, the replacement of $x$ edge 5-6 with a $y$ edge improves synchronization by slightly lowering the synchronization threshold. According to our stability criterion (4.4), this happens due to a slight decrease in the traffic load on the bottleneck edge $b_{23}^x$ (see (5.1)), compared to the original network of Figure 1(a) with all $x$ edges where one additional path $P_{16}$ goes through edge 2-3. As a result, it decreases the contribution of the dominating term $a_x b_k^x$ in (4.4). At the same time, the contribution of the other factors $\omega_y b_k^{int}$ and $\alpha_x^k$ remains insignificant, especially due to the fact that $\alpha_x^k$ still lies on a flat part of the approximating curve (5.4) before this exponential curve takes off at larger values of $b_k^{int}$. On the other hand, such a replacement of the bottleneck node 2-3 in the network of Figure 1(c) significantly increases the intralayer traffic load $b_k^{int}$, requiring infinitely large $\alpha_{23}^x$ to stabilize the stability system (5.2) and causing synchronization to break.

## 6. Synchrony breakdown in larger networks.

To demonstrate that similar synchrony breakdown phenomena occur in larger networks and can be effectively predicted by our method, we consider a 20-node network of Lorenz (and then double-scroll) oscillators described in Figure 4(a). The network is initially coupled entirely through the $x$ variable. To test our prediction that replacing edges with a high traffic load can make the network unsynchronizable, we index the edges according to their $b_k^x$. Edges similar to edge 10-12 have very few paths that pass through them and subsequently have a low $b_k^x$ (and, in turn, $b_k^{int}$, shown as the black curve in Figure 4(c)). We successively replace $x$ edges (denoted by black edges in Figure 4(a)) with $y$ edges (denoted by gray edges in Figure 4(b)) according to this ordering until the network is completely connected through $y$ edges. The values of $b_k^{int}$ range from 0 (for edge 10-12 with edge ranking index 1 (see Figure 4(c)), bypassed by all chosen interlayer paths) to 100–400 for highly loaded edges (for example, for edge 3-5 for which every path from node 3 of the $x$ layer graph to any other node in the $y$ layer must pass through it).

### 6.1. Twenty-node networks of Lorenz oscillators.

The coupling necessary to synchronize the $x$-coupled Lorenz network (3.1) described in Figure 4(a) is $c \approx 86.95$. As outlying, low

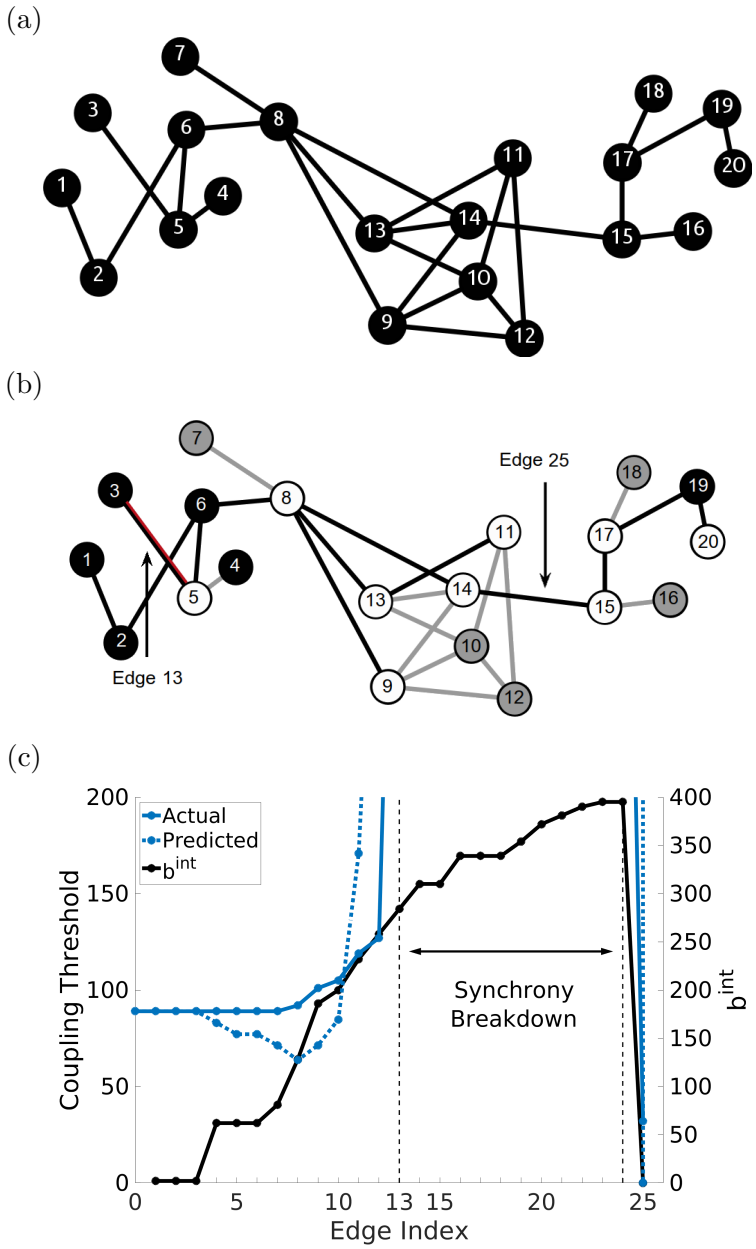


**Figure 4.** *Effect of successively replacing $x$ coupling edges with $y$ coupling edges on synchronization in a 20-node network of Lorenz oscillators (3.1). (a) Original $x$-coupled network before replacing edges according to their traffic load. (b) Snapshot of the multilayer network before the edge 3-5, labeled as the 13th edge according to the traffic load ranking, is replaced. The replacement of this critical edge (red) yields the breakdown of synchronization in the network. Further successive replacement of remaining $x$ edges (gray) with higher traffic load preserves the instability of synchronization, until all 25 edges have been replaced with a $y$ edge, yielding a single-layer $y$-coupled network with $b^{int} = 0$ that is able to synchronize again. (c) Actual (blue solid line) and predicted (blue dotted line) thresholds for the coupling strength required to synchronize the network after the $i$th $x$ edge has been successively replaced with a $y$ edge. The black solid line depicts the interlayer traffic $b^{int}$ for the respective edge. The predicted coupling thresholds are computed from (5.5) using the exponential fit in Figure 3 and scaling factors $\beta = 0.031$ and $\gamma = 0.5993$.*

traffic edges are replaced with $y$ edges, there is almost no effect on the threshold for the coupling strength required to synchronize the network, evidenced by the lack of change in the actual coupling threshold for the first eight edges replaced in Figure 4(c). As successively more loaded edges are replaced in the network (indicated by the dramatic increase in $b^{int}$), the network becomes more difficult to synchronize, until edge 13 (edge 3-5 which is depicted in red in Figure 4(b)) is replaced. Afterward, synchronization is no longer feasible for the network for any additional edge replacement, until edge 25 (edge 14-15 in Figure 4). Replacing edge 25, shown in Figure 4(b), corresponds to finishing the successive edge replacement process, and results in a graph identical to the one in Figure 4(a), but in which all of the edges represent $y$ coupling (gray) instead of $x$ coupling (black). This reinforces our traffic load predictions for the breakdown of synchrony in two ways: (i) after enough highly loaded edges are replaced (even with a normally favorable coupling type), the network can no longer synchronize for *any* coupling strength, and (ii) replacing only one edge that is very highly loaded can make the network unsynchronizable, evidenced by the network having no synchronizing coupling value even when all but one edge has been replaced (see edge index 24 in Figure 4(c)).

As in the six-node example of Figure 1(a), we have obtained a good fit in Figure 4(c) which only focuses on placing the stability conditions on $x$ edges in (4.4), because the stability term $\alpha_x$ required to stabilize the $x$ stability system (5.2) must be significantly higher than $\alpha_y$ in the $y$ stability system (5.2) (compare Figure 3(a)–(b)). We use the same criterion (5.5) with the same constants $a_x$, $\omega_x$, and $\alpha_x^k$ to predict the synchronization threshold and only need to identify the traffic loads $b_k^{int}$ and the scaling factors $\gamma$ and $\beta$ for a better fit, once and for all variations of the multilayer network topologies used in Figure 4(c). In contrast to the six-node network example where traffic load $b_k^{int}$ can be easily calculated by hand as in (5.1), computing $b_k^{int}$ for the 20-node or larger networks is a laborious task which was performed by an algebraic algorithm, implemented as MATLAB code and given in the supplementary materials (M125712_01.zip [local/web 230KB]). While the values of $b_k^{int}$ heavily depend on the choice of paths from one node to another, our algorithm uses the natural choice of the shortest paths, computed via Dijkstra's algorithm [28]. Optimizing the choices of not necessarily shortest paths that distribute traffic loads on edges more equally may yield even better predictions and fits.

**6.2. Networks of double scroll oscillators.** To illustrate the generality of synchrony break phenomenon when "good" but highly loaded links go "bad," we apply our numerically assisted method to networks (2.1), comprised by chaotic double-scroll oscillators [42]

$$\begin{aligned} \dot{x}_i &= \kappa(y_i - x_i - h(x)) + \sum_{j=1}^{n} c_{ij}x_j, \\ \dot{y}_i &= x_i - y_i + z_i + \sum_{j=1}^{n} d_{ij}y_j, \\ \dot{z}_i &= -\lambda y_i - \mu z_i, \quad i = 1, \dots, n, \end{aligned} \tag{6.1}$$

with

$$h(x) = \begin{cases} m_1(x+1) - m_0, & x < -1, \\ m_0 x, & -1 \le x \le 1, \\ m_1(x-1) + m_0, & x > 1, \end{cases}$$

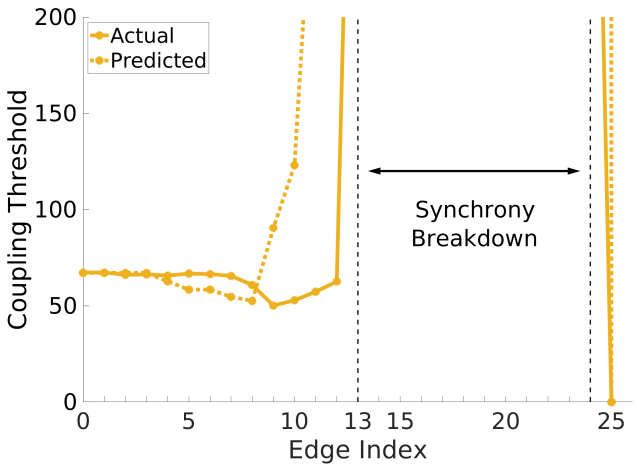


**Figure 5.** *Effect of successively replacing $x$ edges with $y$ edges on the synchronization threshold in a 20-node network of double-scroll oscillators. The network topology, edge replacement process, and notations are identical to those in Figure 4(a)–(b). Notice the same location of critical links (edges 13 to 24) whose replacement leads to synchrony breaks as in the network of Lorenz oscillators (cf. Figure 4(c)).*

and standard parameters $\kappa = 10$, $m_0 = -1.27$, $m_1 = -0.68$, $\lambda = 15$, and $\mu = 0.038$.

Similarly to networks of Lorenz oscillators (3.1), a pair of double-scroll oscillators (6.1) can be synchronized through either the $x$ or $y$ variable, and the minimum coupling strength required for synchronization in a two-node $y$-coupled network, $d^* = 1.16$, is much lower than the coupling threshold in the two-node $x$-coupled network, $c^* = 5.94$.

In Figure 5, we apply our method to predict the synchronization thresholds in the 20-node network of Figure 4 as in the same network of Lorenz oscillators. When successively replacing $x$ edges in the network, there is initially a decrease in the coupling threshold for synchronization, when peripheral edges or edges in highly connected regions of the graph with low traffic loads $b_k^{int}$ are replaced with more favorable $y$ edges that provide better pairwise convergence to synchronization. Then, as with the network of Lorenz oscillators, when edge 13 (edge 3-5) is replaced with a $y$ edge, synchronization is no longer attainable. Synchronization then returns when the entire $x$-coupled network has been replaced with $y$ edges. Notably, the synchrony break occurs at the same edge as in the network of Lorenz oscillators, suggesting that critical edges whose replacement hampers synchronization are mainly controlled by the network multilayer topology rather than the individual properties of the intrinsic oscillators, provided that the oscillators possess similar synchronization properties as the Lorenz and double-scroll oscillators.

The solid curve in Figure 5 displays the synchronization thresholds, calculated via the stability criterion (5.5) with $a_x = 5.94 \times 2 = 11.88$, $\omega_y = 1.0$, $\beta = 0.0095$, $\gamma = 0.282$, and the approximating function $\alpha_x = 1.556 \exp(3.711\beta\omega_y b_k^{int})$ with the same traffic loads $b_k^{int}$ shown in Figure 4. This approximating function is obtained from a stability diagram for coupled double-scroll oscillators which is computed similarly to Figure 3 and displays a similar threshold effect as in Figure 3 [not shown]. As in the Lorenz oscillator case, the auxiliary stability system (4.5) for $\alpha_x$ is much more sensitive to increasing $b_k^{int}$ than the stability system (4.6) for $\alpha_y$;

therefore, one can only evaluate the stability condition (5.5) for the $x$ coupling $c$ to identify a bottleneck for the synchronization threshold in the entire network.

Going back to the puzzle example, we have also performed a similar analysis of the six-node network of Figure 1, where the Lorenz oscillators are replaced with the double-scroll oscillators [not shown]. Remarkably, this analysis indicates the same qualitative phenomena when the replacement of the lightly loaded edge 5-6 slightly lowers the synchronization threshold from $c = 13.57$ in the original $x$-coupled single-layer network of Figure 1(a) to $c = 13.36$ and predicts the breakdown of synchrony when edge 2-3 is replaced as in the Lorenz network.

We have also simulated series of other 20-node networks (3.1) and then networks (6.1) where *all* oscillators were connected via $x$ layer graphs, whereas the $y$ coupling only connected some of the oscillators. In contrast to the networks of Figures 1 and 4, where the critical highly loaded links separate the network into disjoint $x$ and $y$ graph components, these networks do not show the effect of synchrony breaking, as any pair of nodes is coupled directly or indirectly via the $x$ graph such that the coupling strengths $c$ can be made strong enough to stabilize synchronization. However, the synchronization thresholds in such networks depend on the location of added $y$ edges in a nonlinear fashion. In support of this claim, we draw the reader's attention to the six-node example of Figure 1(b), where the $x$ graph connects all six nodes and the replacement of edge 5-6 with a $y$ edge lowers the synchronization threshold. On the contrary, the replacement of the $x$ edge 3-5 with an edge $y$, which still preserves the connectedness of the $x$ graph, increases the synchronization threshold, as predicted by the method (see Figure 1(c)). The 20-node networks with connected $x$ graphs yield similar effects. To avoid repetition, these results are not shown.

**6.3. Networks of Hindmarsh–Rose oscillators.** To convince the reader that the counterintuitive effects of synchrony breaking do not originate from the chaoticity of the oscillators, we have considered a network of limit-cycle Hindmarsh–Rose oscillators [7]:

$$\begin{aligned} \dot{x}_i &= ax_i^2 - y_i - z_i + \sum_{j=1}^{n} c_{ij}x_j, \\ \dot{y}_i &= (a+\alpha)x_i - y_i + \sum_{j=1}^{n} d_{ij}y_j, \\ \dot{z}_i &= \mu(bx_i + c - z_i), \quad i = 1, \dots, n. \end{aligned} \tag{6.2}$$

The individual Hindmarsh–Rose model represents a class of spiking and bursting neurons where $x$ describes the membrane potential, and the variables $y$ and $z$ take into account the transport of ions across the membrane through fast and slow ion channels, respectively. The Hindmarsh–Rose model exhibits periodic square-wave bursting across a wide range of parameters, including the chosen parameters $a = 2.8$, $\alpha = 1.6$, $c = 5$, $b = 9$, $\mu = 0.001$ [9].

While coupling through the $y$ variables does not make physiological sense, we use this network as a phenomenological example of a multilayer network of periodic oscillators which exhibits the same effect of synchrony breaking observed in the networks of chaotic Lorenz and double-scroll oscillators. The analysis of the six-node network of Figure 1, where the chaotic Lorenz oscillators are replaced with the periodic Hindmarsh–Rose oscillators, yields a similar dependence of the synchronization thresholds as a function of the edge replacement

[not shown]. In particular, the threshold coupling for the network of Figure 1(b), where the lightly loaded $x$ edge 5-6 is replaced with a $y$ edge, is $c = 1.66$. However, the replacement of the highly loaded $x$ edge 2-3 (see Figure 1(c)) yields an infinitely large synchronization threshold as in the examples of the Lorenz and double-scroll oscillators. This suggests that the synchronization breakdown effect is not rooted in the particular properties of the chosen limit cycle or chaotic oscillators but rather defined by the structure of a multilayer network and the location of highly loaded links.

**7. Predicting synchrony in large random networks.** Our numerically assisted multilayer connection graph method is also applicable to large, possibly random networks for which the intralayer and interlayer traffic loads can be calculated similarly to the 20-node networks through the MATLAB algebraic algorithm given in the supplementary materials (M125712_01.zip [local/web 230KB]). The algebraic algorithm is rooted in the Dijkstra algorithm, and sorting the shortest paths therefore has a comparable complexity. This complexity along with the required computer power are limitations on the (very large) network size that can be handled by the method. In this regard, predicting synchronization in reasonably large networks of 100–1000 nodes via the stability criterion (5.5) based on the calculations of traffic loads $b_k^x$, $b_k^y$, and $b_k^{int}$ is a simple, computationally inexpensive task, comparable to the application of the connection graph method or master stability function to predicting synchronization in single-layer networks.

Figure 6 demonstrates the actual and predicted synchronization thresholds in 100-node two-layer Erdős–Rényi networks of Lorenz oscillators (3.1). The procedure for constructing these two-layer random networks is as follows. We begin with a single-layer $x$-coupled Erdős–Rényi network whose edges are generated with probability $p = 0.05$. Then we generate five two-layer networks obtained from the 100 random Erdős–Rényi network by replacing 25% of randomly chosen $x$ edges with $y$ edges. These five networks have the same fraction of $x$ and $y$ edges, but the structures of their $x$ and $y$ layers are different (the adjacency lists of their two-layer network topologies are given in the supplementary materials, M125712_01.zip [local/web 230KB]). Figure 6(b) shows that these highly connected networks do not exhibit the synchronization breakdown effect due to the absence of bottleneck edges that would separate the layers and correspond to high interlayer traffic load $b_k^{int}$. Indeed, the maximum traffic load $b_k^{int}$ for the most loaded edge in each of the five networks is nearly the same such that the synchronization thresholds do not vary significantly.

**8. Conclusions.** While the study of synchronization in multilayer dynamical networks has gained significant momentum, the general problem of assessing the stability of synchronization as a function of multilayer network topology remained practically untouched due to the absence of general predictive methods. The existing eigenvalue methods, including the master stability function [49], which effectively predict synchronization thresholds in single-layer networks, cannot be applied to multilayer networks in general. This is due to the fact that the connectivity matrices corresponding to two or more connection layers do not commute in general, and therefore the eigenvalues of the connectivity matrices cannot be used. Therefore, synchronization in multilayer networks is usually studied on a case by case basis either via (i) full-scale simulations of *all* transversal Lyapunov exponents of the $(n-1) \times s$-dimensional system of variational equations [27], where $n$ is the network size and $s$ is the dimension of

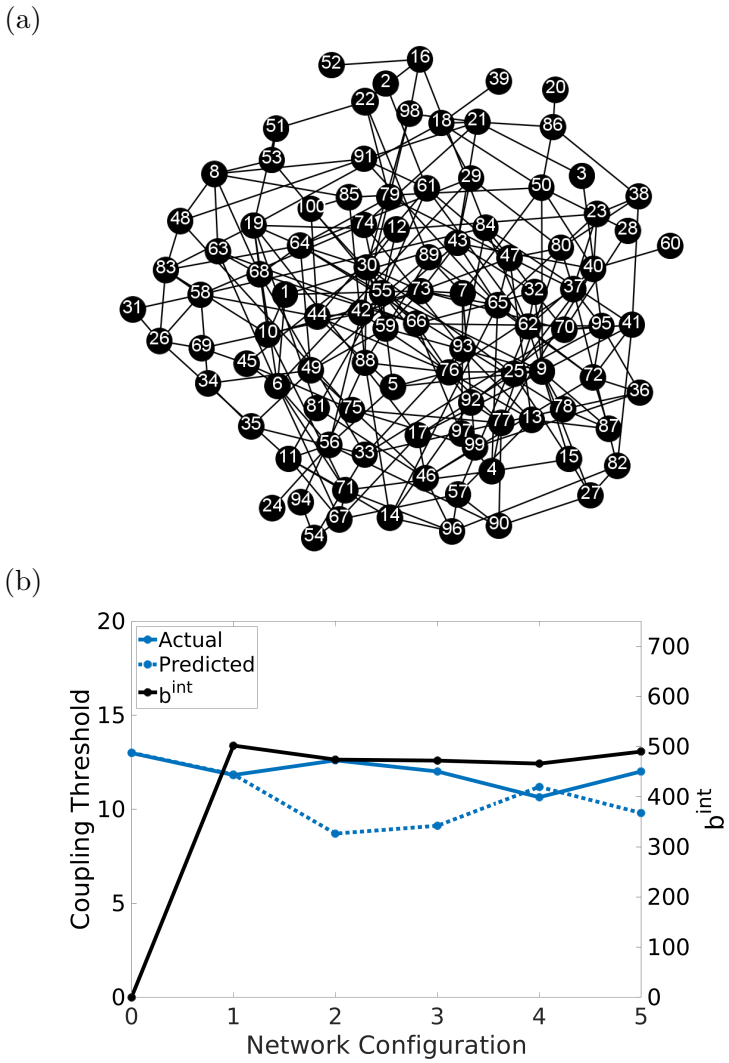


**Figure 6.** *Synchronization in two-layer random Erdős–Rényi networks of* 100 *Lorenz oscillators* (3.1). (a) *Original x-coupled Erdős–Rényi network generated with probability* $p = 0.005$ *for the presence of an x edge.* (b). *Actual (blue solid line) and predicted (blue dotted line) synchronization thresholds in five two-layer network configurations obtained from the* 100 *random Erdős–Rényi network by replacing* 25% *of randomly chosen x edges with y edges. The black solid line depicts the interlayer traffic* $b^{int}$ *for an edge with the highest traffic load. Notice only minor changes in* $b^{int}$ *and, therefore, in the synchronization thresholds in the five two-layer network configurations with the same fraction of x and y edges. Similarly to Figure* 4, *the predicted thresholds are computed from* (5.5) *using the exponential fit in Figure* 3 *and scaling factors* $\beta = 0.012365$ *and* $\gamma = 0.365$.

the intrinsic node dynamics or, more effectively via (ii) simultaneous block diagonalization of the connectivity matrices [36] which in some cases can reduce the problem of assessing synchronization in a large network to a smaller network which, however, contains positive and negative connections, including self-loops such that the exact role of multilayer network

topology and the addition or exchange of edges remains unclear.

In this paper, we have made significant progress in understanding synchronization properties of multilayer networks by developing a predictive method, called the multilayer connection graph method, which does not rely on calculations of eigenvalues of the connectivity matrices and therefore can handle multilayer networks. Originated from the connection graph method for synchronization in single-layer networks [16], our method combines stability theory with graph theoretical reasoning. Two key ingredients of the method are (i) the calculation of stability diagrams for the auxiliary $s$-dimensional system which indicate how the dynamics of the given oscillator comprising the network can be stabilized via one variable corresponding to one connection layer when an instability is introduced via the other variable from another connection layer and (ii) the calculation of traffic loads via a given edge on the multilayer connection graph. All together, these quantities allow for predicting the synchronization threshold and identifying critical links that control synchronization in the original, potentially large multilayer network.

Using the method, we have discovered striking, highly unexpected phenomena not seen in single-layer networks. In particular, we have shown that replacing a link with a light interlayer traffic load by a stronger pairwise converging coupling via another layer may improve synchronizability, as one would expect. At the same time, such a replacement of a highly loaded link may essentially worsen synchronizability and make the network unsynchronizable, turning the pairwise stabilizing "good" link into a destabilizing connection (a "bad" link). The critical links whose replacement can lead to synchrony break are typically the ones that connect the layers such that the oscillators from two layers become coupled through the intrinsic, nonlinear equations of the individual oscillator that correspond to a "relay" node passed by the only path from one layer to the other. As a result, the intrinsic dynamics of the individual node oscillator plays a pivotal role in the stability of synchronization. In this paper, we have limited our attention to Type I limit-cycle and chaotic oscillators such as the Lorenz, double-scroll, and Hindmarsh-Rose oscillators that yield synchronization that remains stable in a single-layer network once the coupling exceeds a critical threshold. Remarkably, when used in a multilayer network, these oscillators have indicated similar synchronization properties, suggesting that the location of critical edges in the considered network may remain unchanged for other Type I oscillators. While our method for assessing synchronization is only applicable to Type I oscillators, it could be modified to handle Type II networks, including multilayer networks of Rössler systems [49]. This modification is a subject of future study.

To gain insight into the determining factors for the emergence of synchrony breaking, without potential confounds associated with the interplay between multiple layers and direction of links, we have considered examples of two-layer undirected networks of identical oscillators. However, the extension of our general method, which was developed for three-layer networks and applied to two-layer networks in this paper, to multiple layers, directed networks, and nonidentical oscillators is fairly straightforward and will be reported elsewhere. In particular, the extension of our method to directed networks can be performed by adapting the generalized connection graph method [5, 6] for single-layer directed networks, where directed edges are symmetrized and assigned additional weights according to the mean node unbalance. In the case of slightly nonidentical oscillators, perfect synchronization cannot exist, but approximate synchronization in multilayer networks is still possible. Our multilayer

connection graph method can be easily extended to such nonidentical oscillators by assessing the stability of a $\delta$-neighborhood of the generating synchronization manifold, similarly to the single-layer connection graph method (see Appendix B in [16]).

Our method can also be modified to handle multilayer neuronal networks connected via electrical, excitatory, and inhibitory synapses which exhibit a number of counterintuitive synergistic effects: when (i) the addition of pairwise repulsive inhibition to single-layer excitatory networks can promote synchronization [13] and (ii) combined electrical and inhibitory coupling can induce synchronization even though each coupling alone promotes an antiphase rhythm [55]. Our method promises to allow an analytical treatment of these effects in large neuronal networks which has been impaired by the absence of predictive methods that can handle excitatory, inhibitory, and electrical neuronal circuitries simultaneously. A key to addressing this issue is the construction of auxiliary stability diagrams that incorporate the variational equations for the stability of the synchronous bursting solution in such networks [13, 55] with the traffic loads on critical links. This study will be reported elsewhere.

**9. Appendix.** In this appendix, we derive the multilayer connection graph method and prove Theorem 4.1. Our goal is to derive the conditions of global asymptotic stability of the synchronization manifold $S$ in the system (2.1). To achieve this goal and develop the stability method, we follow the steps of the proof of the connection graph method [16]. The concept is similar, up to a certain step where a new stability argument is used.

In the network model (2.1), we introduce the difference variable

$$\mathbf{X}_{ij} = \mathbf{x}_j - \mathbf{x}_i, \quad i,j = 1,\dots,n, \tag{9.1}$$

whose convergence to zero will imply the transversal stability of the synchronization manifold $S$.

Subtracting the $i$th equation from the $j$th equation in system (2.1), we obtain the equations for the transversal stability of $S$:

$$\begin{aligned}\dot{\mathbf{X}}_{ij} &= \mathbf{F}(\mathbf{x}_j) - \mathbf{F}(\mathbf{x}_i) + \sum_{k=1}^{n}\{c_{jk}P\mathbf{X}_{jk} - c_{ik}P\mathbf{X}_{ik} \\ &\quad + d_{jk}L\mathbf{X}_{jk} - d_{ik}L\mathbf{X}_{ik} + g_{jk}M\mathbf{X}_{jk} - g_{ik}M\mathbf{X}_{ik}\}, \quad i,j = 1,\dots,n.\end{aligned} \tag{9.2}$$

To obtain the explicit dependence of $\mathbf{F}(\mathbf{x}_j) - \mathbf{F}(\mathbf{x}_i)$ on $\mathbf{X}_{ij}$, we introduce the following vector notation:

$$\mathbf{F}(\mathbf{x}_j) - \mathbf{F}(\mathbf{x}_i) = \left[\int_0^1 D\mathbf{F}(v\mathbf{x}_j + (1-v)\mathbf{x}_i)dv\right]\mathbf{X}_{ij},$$

where $D\mathbf{F}$ is the $3\times 3$ Jacobian matrix of $\mathbf{F}$. This notation is simply a compact form of the mean value theorem, $f(B) - f(A) = f'(C)(B-A)$, applied to the vector functions $\mathbf{F}(\mathbf{x}_j)$ and $\mathbf{F}(\mathbf{x}_i)$, where the Jacobian $D\mathbf{F}$ is evaluated at some point $C \in [\mathbf{x}_i, \mathbf{x}_j]$.

Therefore, the difference system (9.2) can be rewritten in the form

$$\begin{aligned}\dot{\mathbf{X}}_{ij} &= \left[\int_0^1 D\mathbf{F}(v\mathbf{x}_j + (1-v)\mathbf{x}_i)dv\right]\mathbf{X}_{ij} + \sum_{k=1}^{n}\{c_{jk}P\mathbf{X}_{jk} - c_{ik}P\mathbf{X}_{ik} \\ &\quad + d_{jk}L\mathbf{X}_{jk} - d_{ik}L\mathbf{X}_{ik} + g_{jk}M\mathbf{X}_{jk} - g_{ik}M\mathbf{X}_{ik}\}, \quad i,j = 1,\dots,n.\end{aligned} \tag{9.3}$$

The first term in the brackets yields instability via the divergence of trajectories within the individual, possibly chaotic oscillators. The second (summation) term, which represents the contribution of the network connections, may overcome the unstable term, provided that the coupling is strong enough.

Notice that the stability of system (9.3) is redundant, as it contains all possible $(n-1)n/2$ nonzero differences $\mathbf{X}_{ij}$ along with $n$ zero differences $\mathbf{X}_{ii}=0$, which can be disregarded. At the same time, there are only $n-1$ linearly independent differences required to show the convergence between $n$ variables $\mathbf{X}_{ij}$. However, this redundancy property and the consideration of all nonzero $\mathbf{X}_{ij}$ are a key ingredient of our approach, which allows for separating the difference variables later in the stability description, without diagonalizing the connectivity matrices.

We strive to find conditions under which the trivial fixed point $\{\mathbf{X}_{ij}=0,\ i,j=1,\dots,n\}$ of system (9.3) is globally stable. This amounts to finding conditions for global stability of synchronization in the network (2.1).

We introduce the following terms $A_{ij}\mathbf{X}_{ij}$, where $A_{ij}$ is a $3\times 3$ matrix, such that[2]

$$A_{ij}=\begin{cases} a_xP &= \text{diag}(a_x,0,0) \text{ if oscillators } i \text{ and } j \\ & \text{belong to } x \text{ layer } C, \\ a_yL &= \text{diag}(0,a_y,0) \text{ if oscillators } i \text{ and } j \\ & \text{belong to } y \text{ layer } D, \\ a_zM &= \text{diag}(0,0,a_z) \text{ if oscillators } i \text{ and } j \\ & \text{belong to } z \text{ layer } G, \\ K &= \text{diag}(\omega_x,\omega_y,\omega_z) \text{ if oscillators } i \text{ and } j \\ & \text{belong to different layers,} \end{cases} \tag{9.4}$$

where constants $a_x,a_y,a_z,\omega_x,\omega_y,\omega_z$ are to be determined.

We add and subtract additional terms $A_{ij}\mathbf{X}_{ij}$ with matrix $A_{ij}$ defined in (9.4) from the stability system (9.3) and obtain

$$\begin{aligned}\dot{\mathbf{X}}_{ij}= &\left[\int_0^1 D\mathbf{F}(v\mathbf{x}_j+(1-v)\mathbf{x}_i)dv-A_{ij}\right]\mathbf{X}_{ij}+A_{ij}\mathbf{X}_{ij} \\ &+\sum_{k=1}^{n}\{c_{jk}P\mathbf{X}_{jk}-c_{ik}P\mathbf{X}_{ik}+d_{jk}L\mathbf{X}_{jk}-d_{ik}L\mathbf{X}_{ik}+g_{jk}M\mathbf{X}_{jk}-g_{ik}M\mathbf{X}_{ik}\}.\end{aligned} \tag{9.5}$$

The introduction of the terms $A_{ij}\mathbf{X}_{ij}$ allows for obtaining stability conditions of the trivial fixed point $\mathbf{X}_{ij}=0$, $i,j=1,\dots,n$, in two steps. Note that the matrix $-A_{ij}$ contributes to

[2] A different choice of matrix $K$, which takes the values (i) $\text{diag}(\omega_x,\omega_y,0)$ if the path between oscillators $i$ and $j$ is only composed of $x$ and $y$ edges, (ii) $\text{diag}(0,\omega_y,\omega_z)$ if the path between oscillators $i$ and $j$ is only composed of $y$ and $z$ edges, (iii) $\text{diag}(\omega_x,0,\omega_z)$ if the path between oscillators $i$ and $j$ is only composed of $x$ and $z$ edges, and (iv) $\text{diag}(\omega_x,\omega_y,\omega_z)$ if the path between oscillators $i$ and $j$ contains $x$, $y$, and $z$ edges, may yield lower bounds on the coupling thresholds $c_k$, $d_k$, and $g_k$ in the stability criterion (9.31). This is due to the fact that splitting the matrix $K$ into the four matrices may lower the interlayer traffic load on edge $k$, $b_k^{int}$. However, this makes practical applications of the method less convenient, as the more conservative bounds on $b_k^{int}$ can be balanced out by the choice of the scaling parameter $\beta$. Furthermore, one would have to impose additional constraints on $\omega_x$, $\omega_y$, and $\omega_z$ that must be large enough to guarantee that every pair $(\omega_x,\omega_y)$, $(\omega_y,\omega_z)$, and $(\omega_x,\omega_z)$ must yield global synchronization in the corresponding two-node network, as opposed to lower values guaranteed by the triple $(\omega_x,\omega_y,\omega_z)$ used in the matrix $K$ in (9.4).

the stability of the fixed point and can compensate for instabilities induced by eigenvalues with nonnegative real parts of the Jacobian $D\mathbf{F}$. This can be achieved by increasing parameters $a_x, a_y, a_z, \omega_x, \omega_y$, and $\omega_z$. At the same time, the instability originated from its positively definite counterpart, matrix $+A_{ij}$, can be damped by the coupling terms through $c_{ij}$, $d_{ij}$, and $g_{ij}$.

*Step* I. We make the first step by introducing the following auxiliary systems for $i, j = 1, \ldots, n$:

$$\dot{\mathbf{X}}_{ij} = \left[\int_0^1 D\mathbf{F}(v\mathbf{x}_j + (1-v)\mathbf{x}_i)\, dv - A_{ij}\right] \mathbf{X}_{ij}. \tag{9.6}$$

This system is identical to system (9.5), where the coupling terms are removed.

$A_{ij}$ can take four different forms, depending on whether oscillators $i$ and $j$ both belong to the $x$ or $y$ or $z$ graphs, or belong to different graphs, for example, if $i$ belongs to the $x$ graph and $j$ belongs to the $y$ graph (see (9.4)). Therefore, we have four types of auxiliary systems:

$$\dot{\mathbf{X}}_{ij} = \left[\int_0^1 D\mathbf{F}(v\mathbf{x}_j + (1-v)\mathbf{x}_i)\, dv - a_x P\right] \mathbf{X}_{ij} \quad \text{if } i \text{ and } j \text{ both belong to the } x \text{ layer}, \tag{9.7}$$

$$\dot{\mathbf{X}}_{ij} = \left[\int_0^1 D\mathbf{F}(v\mathbf{x}_j + (1-v)\mathbf{x}_i)\, dv - a_y L\right] \mathbf{X}_{ij} \quad \text{if } i \text{ and } j \text{ both belong to the } y \text{ layer}, \tag{9.8}$$

$$\dot{\mathbf{X}}_{ij} = \left[\int_0^1 D\mathbf{F}(v\mathbf{x}_j + (1-v)\mathbf{x}_i)\, dv - a_z M\right] \mathbf{X}_{ij} \quad \text{if } i \text{ and } j \text{ both belong to the } z \text{ layer}, \tag{9.9}$$

$$\dot{\mathbf{X}}_{ij} = \left[\int_0^1 D\mathbf{F}(v\mathbf{x}_j + (1-v)\mathbf{x}_i)\, dv - K\right] \mathbf{X}_{ij} \quad \text{if } i \text{ and } j \text{ belong to different layers}. \tag{9.10}$$

Remarkably, the auxiliary system (9.7) coincides with the difference system for the global stability of synchronization in a two-oscillator network (2.1) with only $x$ coupling, where $a_x$ plays the role of the double coupling strength that guarantees the stability (see [16] for a detailed discussion on this relation).

Similarly, the stability of auxiliary system (9.8) [(9.9)] implies global stability of synchronization in the two-node network (2.1) with only $y$ ($z$) coupling, where $a_y$ ($a_z$) is the double coupling strength of the $y$ ($z$) connection. Last, the stability of auxiliary system (9.10) guarantees globally stable synchronization in the two-node network with all $x, y$, and $z$ coupling, where a combination of constants $\omega_x, \omega_y$, and $\omega_z$, present in $K$, is a combination of the double coupling strengths of $x, y$, and $z$ connections that is sufficient to induce stable synchronization in the $xyz$-coupled two-node network.

Therefore, our immediate goal is to find upper bounds on the values of $a_x$, $a_y$, $a_z$, $\omega_x$, $\omega_y$, and $\omega_z$ that make the origin of the auxiliary systems (9.7)–(9.10) stable. This amounts to proving global synchronization in the four $x$-, $y$-, $z$-, and $xyz$-coupled networks that are composed of two oscillators. As only Type I oscillators [21] are capable of synchronizing globally and retaining synchronization for any coupling strength exceeding some critical threshold, our approach based on the calculation of $a_x$, $a_y$, and $a_z$ is thus limited to this class of oscillators.

The proof of global stability in (9.7)–(9.10) and derivation of bounds $a_x$, $a_y$, $a_z$ and $\omega_x, \omega_y, \omega_z$ involves the construction of a Lyapunov function along with the assumption of the eventual dissipativeness of the coupled system. Therefore, before advancing with the study of larger networks (2.1), one has to prove that globally stable synchronization in the simplest $x$-, $y$-, $z$-, and $xyz$-coupled two-oscillator networks is achievable. The bound $a_x$ for $x$-coupled Lorenz oscillators was given in [16]. Upper bounds for $a_y$, $a_z$, $\omega_x, \omega_y, \omega_z$ can be derived similarly.

Having obtained the bounds $a_x$, $a_y$, $a_z$ and $\omega_x, \omega_y, \omega_z$, and therefore proving the stability of the auxiliary systems (9.7)–(9.10), we can take the second step in analyzing the full stability system (9.5).

*Step* II. The bounds $a_x$, $a_y$, $a_z$ and $\omega_x, \omega_y, \omega_z$ that stabilize the auxiliary systems (9.7)–(9.10) reduce the stability analysis of system (9.5) to the following equations by excluding the term in brackets:

$$\begin{aligned}\dot{\mathbf{X}}_{ij} &= A_{ij}\mathbf{X}_{ij} + \sum_{k=1}^{n}\{c_{jk}P\mathbf{X}_{jk} - c_{ik}P\mathbf{X}_{ik} + d_{jk}L\mathbf{X}_{jk} - d_{ik}L\mathbf{X}_{ik} \\ &\quad + g_{jk}M\mathbf{X}_{jk} - g_{ik}M\mathbf{X}_{ik}\}, \quad i,j = 1,\dots,n.\end{aligned} \tag{9.11}$$

Note that the positive term $A_{ij}\mathbf{X}_{ij}$, which contains the upper bounds $a_x$, $a_y$, $a_z$ and $\omega_x, \omega_y, \omega_z$, is destabilizing and must be compensated for by the coupling terms. To study the stability of (9.11), we introduce a Lyapunov function of the form

$$V = \frac{1}{4}\sum_{i=1}^{n}\sum_{j=1}^{n}\mathbf{X}_{ij}^T \cdot I \cdot \mathbf{X}_{ij}, \tag{9.12}$$

where $I$ is a $3 \times 3$ identity matrix.

Its time derivative with respect to system (9.11) becomes

$$\begin{aligned}\dot{V} &= \tfrac{1}{2}\sum_{i=1}^{n}\sum_{j=1}^{n}\mathbf{X}_{ij}^T A_{ij}\mathbf{X}_{ij} \\ &\quad - \tfrac{1}{2}\sum_{i=1}^{n}\sum_{j=1}^{n}\sum_{k=1}^{n}\{c_{jk}\mathbf{X}_{ji}^T IP\mathbf{X}_{jk} + c_{ik}\mathbf{X}_{ik}^T IP\mathbf{X}_{ij}\} \\ &\quad - \tfrac{1}{2}\sum_{i=1}^{n}\sum_{j=1}^{n}\sum_{k=1}^{n}\{d_{jk}\mathbf{X}_{ji}^T IL\mathbf{X}_{jk} + d_{ik}\mathbf{X}_{ik}^T IL\mathbf{X}_{ij}\} \\ &\quad - \tfrac{1}{2}\sum_{i=1}^{n}\sum_{j=1}^{n}\sum_{k=1}^{n}\{g_{jk}\mathbf{X}_{ji}^T IM\mathbf{X}_{jk} + g_{ik}\mathbf{X}_{ik}^T IM\mathbf{X}_{ij}\}.\end{aligned} \tag{9.13}$$

We need to demonstrate the negative semidefiniteness of the quadratic form $\dot{V}$. As ($\mathbf{X}_{ii}^2 =$

0, $\mathbf{X}_{ij}^2 = \mathbf{X}_{ji}^2$), the first sum simplifies to

$$S_1 = \sum_{i=1}^{n-1} \sum_{j>i}^{n} A_{ij} \mathbf{X}_{ij}^2. \tag{9.14}$$

This sum is always positive definite, and its contribution must be compensated for by the second, third, and fourth sums:

$$\begin{aligned} S_2 &= -\tfrac{1}{2} \sum_{i=1}^{n} \sum_{j=1}^{n} \sum_{k=1}^{n} \{c_{jk} \mathbf{X}_{ji}^T IP \mathbf{X}_{jk} + c_{ik} \mathbf{X}_{ik}^T IP \mathbf{X}_{ij}\}, \\ S_3 &= -\tfrac{1}{2} \sum_{i=1}^{n} \sum_{j=1}^{n} \sum_{k=1}^{n} \{d_{jk} \mathbf{X}_{ji}^T IL \mathbf{X}_{jk} + d_{ik} \mathbf{X}_{ik}^T IL \mathbf{X}_{ij}\} \\ S_4 &= -\tfrac{1}{2} \sum_{i=1}^{n} \sum_{j=1}^{n} \sum_{k=1}^{n} \{g_{jk} \mathbf{X}_{ji}^T IM \mathbf{X}_{jk} + g_{ik} \mathbf{X}_{ik}^T IM \mathbf{X}_{ij}\}. \end{aligned} \tag{9.15}$$

Due to the coupling symmetry, the two terms in $S_2$, $S_3$, and $S_4$ can be made identical by exchanging the indices $i$ with $j$ in the second terms such that

$$\begin{aligned} S_2 &= -\sum_{i=1}^{n} \sum_{j=1}^{n} \sum_{k=1}^{n} c_{jk} \mathbf{X}_{ji}^T IP \mathbf{X}_{jk}, \\ S_3 &= -\sum_{i=1}^{n} \sum_{j=1}^{n} \sum_{k=1}^{n} d_{jk} \mathbf{X}_{ji}^T IL \mathbf{X}_{jk}, \\ S_4 &= -\sum_{i=1}^{n} \sum_{j=1}^{n} \sum_{k=1}^{n} g_{jk} \mathbf{X}_{ji}^T IM \mathbf{X}_{jk}. \end{aligned} \tag{9.16}$$

Taking into account that $\mathbf{X}_{jj} = 0$, we obtain

$$\begin{aligned} S_2 &= -\sum_{i=1}^{n} \sum_{k=1}^{n-1} \sum_{j>k}^{n} c_{jk} \mathbf{X}_{ji}^T IP \mathbf{X}_{jk} - \sum_{i=1}^{n} \sum_{k=1}^{n-1} \sum_{j<k}^{n} c_{jk} \mathbf{X}_{ji}^T IP \mathbf{X}_{jk}, \\ S_3 &= -\sum_{i=1}^{n} \sum_{k=1}^{n-1} \sum_{j>k}^{n} d_{jk} \mathbf{X}_{ji}^T IL \mathbf{X}_{jk} - \sum_{i=1}^{n} \sum_{k=1}^{n-1} \sum_{j<k}^{n} d_{jk} \mathbf{X}_{ji}^T IL \mathbf{X}_{jk}, \\ S_4 &= -\sum_{i=1}^{n} \sum_{k=1}^{n-1} \sum_{j>k}^{n} g_{jk} \mathbf{X}_{ji}^T IM \mathbf{X}_{jk} - \sum_{i=1}^{n} \sum_{k=1}^{n-1} \sum_{j<k}^{n} g_{jk} \mathbf{X}_{ji}^T IM \mathbf{X}_{jk}. \end{aligned} \tag{9.17}$$

Again, exchanging $j$ and $k$ in the second terms of $S_2, S_3$ and $S_4$ and implying the symmetries of coupling $c_{jk} = c_{kj}$, $d_{jk} = d_{kj}$, and $g_{jk} = g_{kj}$, we obtain

$$\begin{aligned} S_2 &= -\sum_{i=1}^{n} \sum_{k=1}^{n-1} \sum_{j>k}^{n} c_{jk} (\mathbf{X}_{ji}^T + \mathbf{X}_{ik}^T) IP \mathbf{X}_{jk}, \\ S_3 &= -\sum_{i=1}^{n} \sum_{k=1}^{n-1} \sum_{j>k}^{n} d_{jk} (\mathbf{X}_{ji}^T + \mathbf{X}_{ik}^T) IL \mathbf{X}_{jk}, \\ S_4 &= -\sum_{i=1}^{n} \sum_{k=1}^{n-1} \sum_{j>k}^{n} g_{jk} (\mathbf{X}_{ji}^T + \mathbf{X}_{ik}^T) IM \mathbf{X}_{jk}. \end{aligned} \tag{9.18}$$

Since $\mathbf{X}_{ji}^T + \mathbf{X}_{ik}^T = \left[\mathbf{x}_i^T - \mathbf{x}_j^T + \mathbf{x}_k^T - \mathbf{x}_i^T\right] = \mathbf{X}_{jk}^T$, we obtain

$$
\begin{aligned}
S_2 &= -\sum_{k=1}^{n-1}\sum_{j>k}^{n} nc_{jk}\mathbf{X}_{jk}^T IP\mathbf{X}_{jk},\\
S_3 &= -\sum_{k=1}^{n-1}\sum_{j>k}^{n} nd_{jk}\mathbf{X}_{jk}^T IL\mathbf{X}_{jk},\\
S_4 &= -\sum_{k=1}^{n-1}\sum_{j>k}^{n} ng_{jk}\mathbf{X}_{jk}^T IM\mathbf{X}_{jk}.
\end{aligned}
\tag{9.19}
$$

Returning to the derivation of the Lyapunov function (9.13) and combining the sums $S_1$, $S_2$, $S_3, S_4$ yields the condition which guarantees that $\dot{V} \le 0$ :

$$
S_1 + S_2 + S_3 + S_4 = \sum_{i=1}^{n-1}\sum_{j>i}^{n} \mathbf{X}_{ij}^T I[A_{ij} - nc_{ij}P - nd_{ij}L - ng_{ij}M]\mathbf{X}_{ij} < 0. \tag{9.20}
$$

The most remarkable property of this condition is that we are able to eliminate the cross terms and formulate the condition in terms of $\mathbf{X}_{ij}$. This is because we chose to consider the redundant system with all possible differences $\mathbf{X}_{ij}$, including linearly dependent ones.

The condition (9.20) finally transforms into

$$
n\sum_{i=1}^{n-1}\sum_{j>i}^{n}[c_{ij}\mathbf{X}_{ij}^T IP\mathbf{X}_{ij} + d_{ij}\mathbf{X}_{ij}^T IL\mathbf{X}_{ij} + g_{ij}\mathbf{X}_{ij}^T IM\mathbf{X}_{ij}] > \sum_{i=1}^{n-1}\sum_{j>i}^{n}\mathbf{X}_{ij}^T IA_{ij}\mathbf{X}_{ij}. \tag{9.21}
$$

Notice that the left-hand side (LHS) of this inequality contains only the differences $\mathbf{X}_{ij}$ between the oscillators that belong to the edges on the connection graphs $C$, $D$, and $G$: the first term on the LHS corresponds to the $x$ layer, the second term is defined by the edges of the $y$ layer, and the third term corresponds to the $z$ layer. At the same time, the variables on the right-hand side (RHS) of (9.21) correspond to all possible differences between pairs of oscillators that might or might not be defined by edges of the connection graphs. Hence, to get rid of the presence of the differences $\mathbf{X}_{ij}$ and therefore find the conditions explicit in the parameters of the network model (2.1), we express the differences on the RHS via the differences on the LHS such that we will be able to cancel them.

So far, we have closely followed the steps in the derivation of the connection graph method [16] for single-layer networks. The inequality (9.21) is similar to that of the connection graph method, except for the presence of the second and third terms on the LHS and a modified matrix $A_{ij}$. A new nontrivial observation, however, is that the total number of oscillators, $n$, in the network (2.1), composed of three connectivity layers, appears as a factor in all three sums on the LHS, corresponding to the $x, y$, and $z$ layers, even though each layer itself may contain fewer oscillators. The stability argument which follows drastically differs from that of the connection graph method.

Denote on the LHS of (9.21) the following: (i) the differences $\mathbf{X}_{ij}$ corresponding to edges of the $x$ graph by $\tilde{\mathbf{X}}_k$, $k = 1, \dots, m$, (ii) the differences $\mathbf{X}_{ij}$ corresponding to edges of the $y$ graph by $\tilde{\mathbf{Y}}_k$, $k = 1, \dots, l$, and (iii) the differences $\mathbf{X}_{ij}$ corresponding to edges of the $z$ graph by $\tilde{\mathbf{Z}}_k$, $k = 1, \dots, q$. Recall that $m, l$, and $q$ are the number of edges on the $x$, $y$, and

$z$ graphs, respectively. In addition, let $X_k$ be a scalar from the vector $\tilde{\mathbf{X}}_k$ which indicates the scalar difference between $x_i$ and $x_j$, corresponding to an edge on the $x$ graph. Similarly, let $Y_k$ ($Z_k$) be a scalar from the vector $\tilde{\mathbf{Y}}_k$ ($\tilde{\mathbf{Z}}_k$) defined by the corresponding $y_i$ and $y_j$ ($z_i$ and $z_j$). Using this notation, the differences $\mathbf{X}_{ij}$ on the RHS will now define the scalars $X_{ij} = x_j - x_i$, $Y_{ij} = y_j - y_i$, and $Z_{ij} = z_j - z_i$. Recall that $(x_i, y_i, z_i)$ are the scalar coordinates of the individual oscillator, composing the network (2.1).

Using this notation, we can rewrite (9.21) as follows:

$$
\begin{aligned}
& n\left[\sum_{k=1}^{m} c_k X_k^2 + \sum_{k=1}^{l} d_k Y_k^2 + \sum_{k=1}^{q} g_k Z_k^2\right] \\
& \quad > a_x \sum_{i=1}^{n-1} \sum_{j>i,(i,j)\in C}^{n} X_{ij}^2 + a_y \sum_{i=1}^{n-1} \sum_{j>i,(i,j)\in D}^{n} Y_{ij}^2 + a_z \sum_{i=1}^{n-1} \sum_{j>i,(i,j)\in G}^{n} Z_{ij}^2 \\
& \quad + \sum_{i=1}^{n-1} \sum_{j>i,(i,j)\notin C,D,G}^{n} [\omega_x X_{ij}^2 + \omega_y Y_{ij}^2 + \omega_z Z_{ij}^2],
\end{aligned}
\tag{9.22}
$$

where $c_k = c_{i_k j_k}$, $d_k = d_{i_k j_k}$, and $g_k = g_{i_k j_k}$. Here, the RHS of (9.22) has four terms obtained by splitting the difference variables into four groups, according to the coefficients of $A_{ij}$ (cf. (9.21) and (9.7)–(9.10)). The first sum on the RHS is composed of the differences that belong to the $x$ graph $C$, the second sum corresponds to the $y$ graph $D$, and the third sum is defined by the $z$ graph $G$, whereas the fourth sum identifies the differences between the oscillators which belong to different graphs such that, for example, $i \in C$ and $j \in D$.

To recalculate the difference variables of the RHS via the variables $X_k$, $Y_k$, and $Z_k$, we should first choose a path from oscillator $i$ to oscillator $j$ for any pair of oscillators $(i, j)$. We denote this path by $P_{ij}$. Its path length $|P_{ij}|$ is the number of edges comprising the path. The important property of the path $P_{ij}$ is that if, for example, it passes through oscillators with indices 1, 2, 3, and 4, then the corresponding difference $X_{14} = x_4 - x_1 = (x_4 - x_3) + (x_3 - x_2) + (x_2 - x_1) = X_{12} + X_{23} + X_{34}$, where the differences $X_{12}, X_{23}$, and $X_{34}$ correspond to the edges and the path length $|P_{14}| = 3$.

The choice of paths is not unique. We typically choose a shortest path between any pair of $i$ and $j$; however, a different choice of paths can yield closer estimates, as discussed in [11] for single-layer networks.

Once the choice of paths is made, we stick with it and begin recalculating the difference variables on the RHS of (9.22) via $X_k$, $Y_k$, and $Z_k$. A potential problem is that we have to deal not with the variables $X_{ij}$, but with their squares $X_{ij}^2$, coming from the calculations of the derivative of the Lyapunov function (9.13). To mitigate this issue, we apply the Cauchy–Schwarz inequality; applied to the above example, it yields $X_{14}^2 = (X_{12} + X_{23} + X_{34})^2 \le 3(X_{12}^2 + X_{23}^2 + X_{34}^2)$. Notice the appearance of the factor 3, indicating the number of edges

comprising the path. Similarly, for any difference $X_{ij}$, $Y_{ij}$, and $Z_{ij}$, we have

$$\begin{aligned} X_{ij}^2 &= \left(\sum_{k\in P_{ij}} X_k\right)^2 \le |P_{ij}| \sum_{k\in P_{ij}} X_k^2, \\ Y_{ij}^2 &= \left(\sum_{k\in P_{ij}} Y_k\right)^2 \le |P_{ij}| \sum_{k\in P_{ij}} Y_k^2, \\ Z_{ij}^2 &= \left(\sum_{k\in P_{ij}} Z_k\right)^2 \le |P_{ij}| \sum_{k\in P_{ij}} Z_k^2, \end{aligned} \tag{9.23}$$

where once again $|P_{ij}|$ indicates the length of the chosen path from oscillator $i$ to oscillator $j$ along the connection graph, a combination of the $x$ and $y$ graphs. At this point, we do not differentiate between paths containing only $x$, $y$, or $z$ edges, but we have to consider interlayer paths when necessary.

Applying this idea to each difference variable on the RHS of (9.22), we obtain the following condition:

$$\begin{aligned} n\left[\sum_{k=1}^{m} c_k X_k^2 + \sum_{k=1}^{l} d_k Y_k^2 + \sum_{k=1}^{q} g_k Z_k^2\right] &> \sum_{k=1}^{m} [a_x b_k^x + \omega_x b_k^{int}] X_k^2 \\ &+ \sum_{k=1}^{l} [a_y b_k^y + \omega_y b_k^{int}] Y_k^2 + \sum_{k=1}^{q} [a_z b_k^z + \omega_z b_k^{int}] Z_k^2 \\ &+ \sum_{k\in D\cup G} [\omega_x b_k^{int}] X_k^2 + \sum_{k\in C\cup G} [\omega_y b_k^{int}] Y_k^2 + \sum_{k\in C\cup D} [\omega_z b_k^{int}] Z_k^2, \end{aligned} \tag{9.24}$$

where $b_k^x = \sum_{j>i;\, k\in P_{ij}\in C}^{n} |P_{ij}|$ is the sum of the lengths of all chosen paths which belong to the $x$ graph $C$ and go through a given $x$ edge $k$. Similarly, $b_k^y = \sum_{j>i;\, k\in P_{ij}\in D}^{n} |P_{ij}|$ ($b_k^z = \sum_{j>i;\, k\in P_{ij}\in G}^{n} |P_{ij}|$) is the sum of the lengths of all chosen paths which belong to the $y$ graph $D$ ($z$ graph $G$) and go through a given $y$ ($z$) edge $k$. Finally, $b_k^{int} = \sum_{j>i;\, k\in P_{ij}:(i,j)\notin C,D,G} |P_{ij}|$ is the sum of the lengths of all chosen paths between pairs of nodes $i$ and $j$ which belong to two different graphs and are composed from more than one type of edge and go through a given edge $k$ which may be an $x$, $y$, or $z$ edge.

Note that the three sums on the LHS of (9.24) correspond to the first three sums on the RHS. In the simplest case where all three $C$, $D$, and $G$ graphs are connected such that each graph couples all $n$ oscillators, $b_k^{int}$ can always be set to 0 since there are always paths between any two nodes that entirely belong to any of the three $x$, $y$, or $z$ graphs. As a result, the last three sums on the RHS disappear, and we immediately obtain the stability conditions by dropping the summation signs and the difference variables:

$$c_k + d_k + g_k > \frac{1}{n}\left\{a_x b_k^x + a_y b_k^y + a_z b_k^z\right\}. \tag{9.25}$$

In the case of disconnected graphs $C$, $D$, and $G$ where all oscillators are coupled through a combination of two or three graphs and $b_k^{int}$ is nonzero, at least two of the last three sums are always present on the RHS. This makes the argument much more complicated but yields

a number of surprising implications of the stability method to specific networks discussed in sections 5 and 6.

A major stability problem, associated with the last three terms, is rooted in the fact that, for example, the fourth sum $\sum_{k\in D\cup G}[\omega_x b_k^{int}]X_k^2$ contains the difference variables $X_k$ that correspond to the edges of the $y$ or $z$ graph. As a result, the first sum $n\sum_{k=1}^{m} c_k X_k^2$ on the LHS, which contains the variables $X_k$ that correspond to $x$ edges, cannot compensate for the fourth sum on the RHS, as they belong to different graphs and therefore cannot be compared. At the same time, the second (third) sum $n\sum_{k=1}^{l} d_k Y_k^2$ $\left(n\sum_{k=1}^{q} g_k Z_k^2\right)$ on the LHS does belong to the $y$ $(z)$ graph but contains the variables $Y_k$ $(Z_k)$ and not $X_k$ needed to handle the fourth sum on the RHS. The same problem relates to the last two sums $\sum_{k\in C\cup G}[\omega_y b_k^{int}]Y_k^2$ and $\sum_{k\in C\cup D}[\omega_z b_k^{int}]Z_k^2$ which contain $Y_k$ and $Z_k$ variables, respectively, and correspond to the "wrong" graphs.

How can we get around this problem? We simply do not have means on the LHS to compensate for the troublesome sums on the RHS. A solution comes from economics: if you do not have means, borrow them! [But act responsibly]. This remark is added to entertain the reader that might be tired of following the proof up to this point.

In fact, the only place to "borrow" these terms from is the auxiliary stability systems (9.7), (9.8), and (9.9), as they do contain the desired variables $X_k$, $Y_k$, and $Z_k$, corresponding to the "right" graphs (the $x$, $y$, and $z$ graphs, respectively). Therefore, we need to go back and modify the auxiliary systems (9.7), (9.8), and (9.9) as follows:

$$\begin{aligned}\dot{\mathbf{X}}_{ij} &= \left[\int_0^1 D\mathbf{F}(v\mathbf{x}_j+(1-v)\mathbf{x}_i)\,dv-[a_x+\alpha_x^k]P\right.\\ &\left.+\omega_y b_k^{int}L+\omega_z b_k^{int}M\right]\mathbf{X}_{ij}\quad \text{if } i,j\in x\text{-edge } k,\end{aligned}\tag{9.26}$$

$$\begin{aligned}\dot{\mathbf{X}}_{ij} &= \left[\int_0^1 D\mathbf{F}(v\mathbf{x}_j+(1-v)\mathbf{x}_i)\,dv-(a_y+\alpha_y^k)L+\right.\\ &\left.\omega_x b_k^{int}P+\omega_z b_k^{int}M\right]\mathbf{X}_{ij}\quad \text{if } i,j\in y\text{-edge } k,\end{aligned}\tag{9.27}$$

$$\begin{aligned}\dot{\mathbf{X}}_{ij} &= \left[\int_0^1 D\mathbf{F}(v\mathbf{x}_j+(1-v)\mathbf{x}_i)\,dv-(a_z+\alpha_z^k)G+\right.\\ &\left.\omega_x b_k^{int}P+\omega_y b_k^{int}L\right]\mathbf{X}_{ij}\quad \text{if } i,j\in z\text{-edge } k.\end{aligned}\tag{9.28}$$

The addition of positive terms $\omega_y b_k^{int}L\mathbf{X}_{ij}$ and $\omega_z b_k^{int}M\mathbf{X}_{ij}$ to the auxiliary system (9.26) worsens its stability; therefore, we have to introduce an additional parameter $\alpha_x^k$ and make sure that it is sufficiently large to stabilize the new auxiliary system. A very important property is that, in (9.26), we have to add the positive, destabilizing term $\omega_y b_k^{int}LX_{ij}$ to the second equation for the $(y_j-y_i)$ difference and the positive, destabilizing term $\omega_z b_k^{int}MX_{ij}$ to the third equation for the $(z_j-z_i)$ difference but try to stabilize the system via increasing the additional parameter $\alpha_x^k$ in the first equation for the $(x_j-x_i)$ equation (note the different inner

matrices: $P$ versus $L$ and $M$ in (9.26)). Depending on the individual oscillator, chosen as the individual unit, this might not be possible, especially when traffic load $b_k^{int}$ on the edge $k$ is high. This property is discussed in detail for the Lorenz and double-scroll oscillator examples in sections 5 and 6. A similar argument carries over to the auxiliary systems (9.27) and (9.28), where, for example, in (9.27) we add the destabilizing terms $\omega_x b_k^{int} P\mathbf{X}_{ij}$ and $\omega_z b_k^{int} M\mathbf{X}_{ij}$ to the $(x_j - x_i)$ and $(z_j - z_i)$ equations, respectively, but seek to stabilize the system via the additional parameter $\alpha_y^k$ in the $(y_j - y_i)$ equation.

Notice that we only modify the auxiliary systems for the existing $x$, $y$, and $z$ edges. All the other auxiliary systems for $\mathbf{X}_{ij}$, which do not correspond to edges of any of the $x$, $y$, or $z$ graphs, remain intact and defined via the original systems (9.7)–(9.10). Thus, the modifications of (9.26), (9.27), and (9.28) make the troublesome sums $\sum_{k\in D\cup G}[\omega_x b_k^{int}]X_k^2$, $\sum_{k\in C\cup G}[\omega_y b_k^{int}]Y_k^2$, and $\sum_{k\in C\cup D}[\omega_z b_k^{int}]Z_k^2$ in (9.24) disappear at the expense of worsened stability conditions of the corresponding auxiliary systems, which is reflected by the appearance of additional terms with $\alpha_x^k$, $\alpha_y^k$, and $\alpha_z^k$. Therefore, (9.24) turns into

$$
\begin{aligned}
n\left[\sum_{k=1}^{m} c_k X_k^2 + \sum_{k=1}^{l} d_k Y_k^2 + \sum_{k=1}^{q} g_k Z_k^2\right] &> \sum_{k=1}^{m}[a_x b_k^x + \omega_x b_k^{int} + \alpha_x^k]X_k^2 \\
&+ \sum_{k=1}^{l}[a_y b_k^y + \omega_y b_k^{int} + \alpha_y^k]Y_k^2 + \sum_{k=1}^{q}[a_z b_k^z + \omega_z b_k^{int} + \alpha_z^k]Z_k^2.
\end{aligned} \tag{9.29}
$$

Notice the new stabilizing constants $\alpha_x^k$, $\alpha_y^k$, and $\alpha_z^k$. Depending on the individual oscillator dynamics and traffic load on edge $k$, these constants might have to be very large or even infinite.

Comparing the terms containing $X_k$, $Y_k$, and $Z_k$ on the LHS and RHS of (9.29) and omitting the summation signs, we obtain the following conditions:

$$
\begin{aligned}
nc_k X_k^2 &> [a_x b_k^x + \omega_x b_k^{int} + \alpha_x^k]X_k^2, \quad k = 1, \dots, m, \\
nd_k Y_k^2 &> [a_y b_k^y + \omega_y b_k^{int} + \alpha_y^k]Y_k^2, \quad k = 1, \dots, l, \\
ng_k Z_k^2 &> [a_z b_k^z + \omega_z b_k^{int} + \alpha_z^k]Z_k^2, \quad k = 1, \dots, q.
\end{aligned} \tag{9.30}
$$

Finally, we omit the difference variables to obtain the bounds on coupling strengths, $c_k$ for $x$ edges, $d_k$ for $y$ edges, and $g_k$ for $z$ edges, sufficient to make the derivative of the Lyapunov function (9.13) negative semidefinite, and therefore ensure global stability of synchronization in the network (2.1). It follows from (9.30) that these upper bounds are

$$
\begin{aligned}
c_k &> \tfrac{1}{n}[a_x b_k^x + \omega_x b_k^{int} + \alpha_x^k], \quad k = 1, \dots, m, \\
d_k &> \tfrac{1}{n}[a_y b_k^y + \omega_y b_k^{int} + \alpha_y^k], \quad k = 1, \dots, l, \\
g_k &> \tfrac{1}{n}[a_z b_k^z + \omega_z b_k^{int} + \alpha_z^k], \quad k = 1, \dots, q.
\end{aligned} \tag{9.31}
$$

This completes the proof of Theorem 4.1. ∎

## REFERENCES

[1] J. Aguirre, R. Sevilla-Escoboza, R. Gutiérrez, D. Papo, and J. M. Buldú, *Synchronization of interconnected networks: The role of connector nodes*, Phys. Rev. Lett., 112 (2014), 248701.

[2] R. Albert and A.-L. Barabási, *Statistical mechanics of complex networks*, Rev. Modern Phys., 74 (2002), pp. 47–97.
[3] M. Barahona and L. M. Pecora, *Synchronization in small-world systems*, Phys. Rev. Lett., 89 (2002), 054101.
[4] I. Belykh, V. Belykh, and M. Hasler, *Blinking model and synchronization in small-world networks with a time-varying coupling*, Phys. D, 195 (2004), pp. 188–206.
[5] I. Belykh, V. Belykh, and M. Hasler, *Generalized connection graph method for synchronization in asymmetrical networks*, Phys. D, 224 (2006), pp. 42–51.
[6] I. Belykh, V. Belykh, and M. Hasler, *Synchronization in asymmetrically coupled networks with node balance*, Chaos, 16 (2006), 015102.
[7] I. Belykh, E. de Lange, and M. Hasler, *Synchronization of bursting neurons: What matters in the network topology*, Phys. Rev. Lett., 94 (2005), 188101.
[8] I. Belykh, M. di Bernardo, J. Kurths, and M. Porfiri, *Evolving dynamical networks*, Phys. D, 267 (2014), pp. 1–6.
[9] I. Belykh and M. Hasler, *Mesoscale and clusters of synchrony in networks of bursting neurons*, Chaos, 21 (2011), 016106.
[10] I. Belykh, M. Hasler, and V. Belykh, *When symmetrization guarantees synchronization in directed networks*, Internat. J. Bifur. Chaos Appl. Sci. Engrg., 17 (2007), pp. 3387–3395.
[11] I. Belykh, M. Hasler, M. Lauret, and H. Nijmeijer, *Synchronization and graph topology*, Internat. J. Bifur. Chaos Appl. Sci. Engrg., 15 (2005), pp. 3423–3433.
[12] I. Belykh, R. Jeter, and V. Belykh, *Foot force models of crowd dynamics on a wobbly bridge*, Sci. Adv., 3 (2017), e1701512.
[13] I. Belykh, R. Reimbayev, and K. Zhao, *Synergistic effect of repulsive inhibition in synchronization of excitatory networks*, Phys. Rev. E (3), 91 (2015), 062919.
[14] I. Belykh and A. Shilnikov, *When weak inhibition synchronizes strongly desynchronizing networks of bursting neurons*, Phys. Rev. Lett., 101 (2008), 078102.
[15] I. V. Belykh, R. Jeter, and V. N. Belykh, *Bistable gaits and wobbling induced by pedestrian-bridge interactions*, Chaos, 26 (2016), 116314.
[16] V. N. Belykh, I. V. Belykh, and M. Hasler, *Connection graph stability method for synchronized coupled chaotic systems*, Phys. D, 195 (2004), pp. 159–187.
[17] V. N. Belykh, N. N. Verichev, L. Kocarev, and L. Chua, *On chaotic synchronization in a linear array of Chua's circuits*, J. Circuits Syst. Comput., 3 (1993), pp. 579–590.
[18] K. A. Blaha, K. Huang, F. Della Rossa, L. Pecora, M. Hossein-Zadeh, and F. Sorrentino, *Cluster synchronization in multilayer networks: A fully analog experiment with LC oscillators with physically dissimilar coupling*, Phys. Rev. Lett., 122 (2019), 014101.
[19] S. Boccaletti, G. Bianconi, R. Criado, C. I. Del Genio, J. Gómez-Gardenes, M. Romance, I. Sendina-Nadal, Z. Wang, and M. Zanin, *The structure and dynamics of multilayer networks*, Phys. Rep., 544 (2014), pp. 1–122.
[20] S. Boccaletti, J. Kurths, G. Osipov, D. L. Valladares, and C. S. Zhou, *The synchronization of chaotic systems*, Phys. Rep., 366 (2002), pp. 1–101.
[21] S. Boccaletti, V. Latora, Y. Moreno, M. Chavez, and D.-U. Hwang, *Complex networks: Structure and dynamics*, Phys. Rep., 424 (2006), pp. 175–308.
[22] J. Buck and E. Buck, *Synchronous fireflies*, Sci. Amer., 234 (1976), pp. 74–85.
[23] S. V. Buldyrev, R. Parshani, G. Paul, H. E. Stanley, and S. Havlin, *Catastrophic cascade of failures in interdependent networks*, Nature, 464 (2010), pp. 1025–1028.
[24] G. Chen and Y. Xinghuo, *Chaos Control Theory and Applications*, Lecture Notes in Control and Inform. Sci. 292, Springer, Berlin, Heidelberg, 2003.
[25] J. J. Collins and I. N. Stewart, *Coupled nonlinear oscillators and the symmetries of animal gaits*, J. Nonlinear Sci., 3 (1993), pp. 349–392.
[26] M. De Domenico, C. Granell, M. A. Porter, and A. Arenas, *The physics of spreading processes in multilayer networks*, Nat. Phys., 12 (2016), pp. 901–906.
[27] C. I. del Genio, J. Gómez-Gardeñes, I. Bonamassa, and S. Boccaletti, *Synchronization in networks with multiple interaction layers*, Sci. Adv., 2 (2016), e1601679.
[28] E. W. Dijkstra, *A note on two problems in connexion with graphs*, Numer. Math., 1 (1959), pp. 269–271.

[29] B. Eckhardt, E. Ott, S. H. Strogatz, D. M. Abrams, and A. McRobie, *Modeling walker synchronization on the Millennium Bridge*, Phys. Rev. E (3), 75 (2007), 021110.
[30] L. Glass and M. C. Mackey, *From Clocks to Chaos: The Rhythms of Life*, Princeton University Press, Princeton, NJ, 1988.
[31] O. Golovneva, R. Jeter, I. Belykh, and M. Porfiri, *Windows of opportunity for synchronization in stochastically coupled maps*, Phys. D, 340 (2017), pp. 1–13.
[32] M. R. Guevara, A. Shrier, and L. Glass, *Phase-locked rhythms in periodically stimulated heart cell aggregates*, Am. J. Physiol. Heart Circ. Physiol., 254 (1988), pp. H1–H10.
[33] J. F. Heagy, L. M. Pecora, and T. L. Carroll, *Short wavelength bifurcations and size instabilities in coupled oscillator systems*, Phys. Rev. Lett., 74 (1995), pp. 4185–4188.
[34] J. L. Hindmarsh and R. M. Rose, *A model of neuronal bursting using three coupled first order differential equations*, Philos. Trans. R. Soc. Lond., B, Biol. Sci., 221 (1984), pp. 87–102.
[35] J. Honerkamp, *The heart as a system of coupled nonlinear oscillators*, J. Math. Biol., 18 (1983), pp. 69–88.
[36] D. Irving and F. Sorrentino, *Synchronization of dynamical hypernetworks: Dimensionality reduction through simultaneous block-diagonalization of matrices*, Phys. Rev. E (3), 86 (2012), 056102.
[37] R. Jeter and I. Belykh, *Synchronization in on-off stochastic networks: Windows of opportunity*, IEEE Trans. Circuits Syst. I, Reg. Papers, 62 (2015), pp. 1260–1269.
[38] M. Kivelä, A. Arenas, M. Barthelemy, J. P. Gleeson, Y. Moreno, and M. A. Porter, *Multilayer networks*, J. Complex Netw., 2 (2014), pp. 203–271.
[39] N. Kopell and B. Ermentrout, *Chemical and electrical synapses perform complementary roles in the synchronization of interneuronal networks*, Proc. Natl. Acad. Sci. USA, 101 (2004), pp. 15482–15487.
[40] Z. Li and G. Chen, *Global synchronization and asymptotic stability of complex dynamical networks*, IEEE Trans. Circuits Syst., II, Exp. Briefs, 53 (2006), pp. 28–33.
[41] E. N. Lorenz, *Deterministic nonperiodic flow*, J. Atmospheric Sci., 20 (1963), pp. 130–141.
[42] R. N. Madan, *Chua's Circuit: A Paradigm for Chaos*, World Scientific, Singapore, 1993.
[43] A. E. Motter, S. A. Myers, M. Anghel, and T. Nishikawa, *Spontaneous synchrony in power-grid networks*, Nat. Phys., 9 (2013), pp. 191–197.
[44] H. Nakao, T. Yanagita, and Y. Kawamura, *Phase-reduction approach to synchronization of spatiotemporal rhythms in reaction-diffusion systems*, Phys. Rev. X, 4 (2014), 021032.
[45] T. I. Netoff and S. J. Schiff, *Decreased neuronal synchronization during experimental seizures*, J. Neurosci., 22 (2002), pp. 7297–7307.
[46] M. E. J. Newman, *The structure and function of complex networks*, SIAM Rev., 45 (2003), pp. 167–256, https://doi.org/10.1137/S003614450342480.
[47] T. Nishikawa and A. E. Motter, *Network synchronization landscape reveals compensatory structures, quantization, and the positive effect of negative interactions*, Proc. Natl. Acad. Sci. USA, 107 (2010), pp. 10342–10347.
[48] T. Nishikawa, J. Sun, and A. E. Motter, *Sensitive dependence of optimal network dynamics on network structure*, Phys. Rev. X, 7 (2017), 041044.
[49] L. M. Pecora and T. L. Carroll, *Master stability functions for synchronized coupled systems*, Phys. Rev. Lett., 80 (1998), pp. 2109–2112.
[50] A. Pikovsky, M. Rosenblum, and J. Kurths, *Synchronization: A Universal Concept in Nonlinear Sciences*, Cambridge Nonlinear Sci. 12, Cambridge University Press, Cambridge, UK, 2003.
[51] M. Porfiri and I. Belykh, *Memory matters in synchronization of stochastically coupled maps*, SIAM J. Appl. Dyn. Syst., 16 (2017), pp. 1372–1396, https://doi.org/10.1137/17M111136X.
[52] M. Porfiri and D. J. Stilwell, *Consensus seeking over random weighted directed graphs*, IEEE Trans. Automat. Control, 52 (2007), pp. 1767–1773.
[53] M. Porfiri, D. J. Stilwell, E. M. Bollt, and J. D. Skufca, *Random talk: Random walk and synchronizability in a moving neighborhood network*, Phys. D, 224 (2006), pp. 102–113.
[54] F. Radicchi and G. Bianconi, *Redundant interdependencies boost the robustness of multiplex networks*, Phys. Rev. X, 7 (2017), 011013.
[55] R. Reimbayev, K. Daley, and I. Belykh, *When two wrongs make a right: Synchronized neuronal bursting from combined electrical and inhibitory coupling*, Philos. Trans. Roy. Soc. A, 375 (2017), 20160282.

[56] P. So, B. C. Cotton, and E. Barreto, *Synchronization in interacting populations of heterogeneous oscillators with time-varying coupling*, Chaos, 18 (2008), 037114.
[57] F. Sorrentino, *Synchronization of hypernetworks of coupled dynamical systems*, New J. Phys., 14 (2012), 033035.
[58] F. Sorrentino and E. Ott, *Adaptive synchronization of dynamics on evolving complex networks*, Phys. Rev. Lett., 100 (2008), 114101.
[59] S. H. Strogatz, *Exploring complex networks*, Nature, 410 (2001), pp. 268–276.
[60] S. H. Strogatz, D. M. Abrams, A. McRobie, B. Eckhardt, and E. Ott, *Theoretical mechanics: Crowd synchrony on the Millennium Bridge*, Nature, 438 (2005), pp. 43–44.
[61] J. Sun, E. M. Bollt, and T. Nishikawa, *Master stability functions for coupled nearly identical dynamical systems*, Europhys. Lett., 85 (2009), 60011.
[62] D. Taylor, S. Shai, N. Stanley, and P. J. Mucha, *Enhanced detectability of community structure in multilayer networks through layer aggregation*, Phys. Rev. Lett., 116 (2016), 228301.
[63] V. Torre, *A theory of synchronization of heart pace-maker cells*, J. Theoret. Biol., 61 (1976), pp. 55–71.
[64] X. F. Wang and G. Chen, *Synchronization in scale-free dynamical networks: Robustness and fragility*, IEEE Trans. Circuits Syst. I, Fundam. Theory Appl., 49 (2002), pp. 54–62.
[65] C. W. Wu, *Synchronization in Coupled Chaotic Circuits and Systems*, World Sci. Nonlinear Sci. A 41, World Scientific, Singapore, 2002.
[66] C. W. Wu, *Synchronization and convergence of linear dynamics in random directed networks*, IEEE Trans. Automat. Control, 51 (2006), pp. 1207–1210.
[67] C. W. Wu and L. O. Chua, *On a conjecture regarding the synchronization in an array of linearly coupled dynamical systems*, IEEE Trans. Circuits Syst. I, Fundam. Theory Appl., 43 (1996), pp. 161–165.
[68] L. Zhang, A. E. Motter, and T. Nishikawa, *Incoherence-mediated remote synchronization*, Phys. Rev. Lett., 118 (2017), 174102.
[69] X. Zhang, S. Boccaletti, S. Guan, and Z. Liu, *Explosive synchronization in adaptive and multilayer networks*, Phys. Rev. Lett., 114 (2015), 038701.